DOE/ER01198/1340

T 1C

MASTER

CHARACTERIZATION OF INTERNAL BOUNDARY LAYER CAPACITORS BASED UPON BARIUM TITANATE AND STRONTIUM TITANATE

BY

HYUN DUK PARK

B.S., Hanyang University, 1974
M.S., University of Illinois at Urbana-Champaign, 1978

DISCLAIMER

This book was prepared as an account of work sponsored by an agency of the United States Government. Neither the United States Government nor any agency thereof, nor any of their employees, makes any warranty, express or implied, or assumes any legal liability or responsibility for the accuracy, completeness, or usefulness of any information, apparatus, product, or process disclosed, or represents that its use would not infringe privately owned rights. Reference herein to any specific commercial product, process, or service by trade name, trademark, manufacturer, or otherwise, does not necessarily constitute or imply its endorsement, recommendation, or favoring by the United States Government or any agency thereof. The views and opinions of authors expressed herein do not necessarily state or reflect those of the United States Government or any agency thereof.

THESIS

Submitted in partial fulfillment of the requirements
for the degree of Doctor of Philosophy in Ceramic Engineering
in the Graduate College of the
University of Illinois at Urbana-Champaign, 1981

Urbana, Illinois

DISTRIBUTION OF THIS DOCUMENT IS UNLIMITED

DISCLAIMER

This report was prepared as an account of work sponsored by an agency of the United States Government. Neither the United States Government nor any agency Thereof, nor any of their employees, makes any warranty, express or implied, or assumes any legal liability or responsibility for the accuracy, completeness, or usefulness of any information, apparatus, product, or process disclosed, or represents that its use would not infringe privately owned rights. Reference herein to any specific commercial product, process, or service by trade name, trademark, manufacturer, or otherwise does not necessarily constitute or imply its endorsement, recommendation, or favoring by the United States Government or any agency thereof. The views and opinions of authors expressed herein do not necessarily state or reflect those of the United States Government or any agency thereof.

DISCLAIMER

Portions of this document may be illegible in electronic image products. Images are produced from the best available original document.

CHARACTERIZATION OF INTERNAL BOUNDARY LAYER CAPACITORS BASED UPON $BaTiO_3$ AND $SrTiO_3$

Hyun Duk Park, Ph.D.
Department of Ceramic Engineering
University of Illinois at Urbana-Champaign, 1981

The properties of polycrystalline electrical ceramics are greatly influenced by the electrical and mechanical boundary conditions existing at grain and phase boundaries. The dielectric properties of internal boundary layer capacitor are directly related to their microstructure, in which semiconducting grains are surrounded by continuously connected thin insulating boundaries. Heterogeneous distributions in resistivity, between conducting grains and insulating boundaries, results in thin, interfacial space charge layers of high capacitance and high apparent dielectric constant.

The nature of ceramic microstructure and the electrical properties of individual grains and junctions was determined by STEM, microprobe analysis and microscale electrical measurements. The chemical compositions of the resistive boundary regions were different from those of the grains. Additives were concentrated in the boundary regions, forming resistive layers. Limited diffusion of the counterdopants into the grain subsurface formed an interfacial compensation layer between the insulating intergranular layer and the semiconducting grains. The electrical behavior of this intermediate layer was found to be similar to that of a depletion layer.

Ceramic microstructures were approximated by a three-layer n-c-i-c-n model and representive equivalent circuit, which was

used to explain the voltage dependence of the dielectric constant and dispersion behavior. Calculated properties were in good agreement with experimental values. Fine grain microstructures developed by liquid phase sintering techniques, were suitable for high dielectric constant multilayer capacitors, based upon internal boundary layer phenomena, and these capacitors had stable dielectric characteristics.

ACKNOWLEDGMENTS

The author expresses his sincere appreciation to his advisor, Dr. David A. Payne for his guidance, encouragement, and enlightening discussions. The author also gratefully acknowledges the help of Dr. S. M. Park, C.T.A. Suchicital and I. D. Ward.

This work was supported by the Transelco Division of Ferro Corporation and by the U.S. Department of Energy under Contract DE-AC02-76ER01198.

TABLE OF CONTENTS

TABLE OF CONTENTS (cont.)

LIST OF TABLES

THIS PAGE

WAS INTENTIONALLY

LEFT BLANK

LIST OF FIGURES

LIST OF FIGURES (cont.)

LIST OF FIGURES (cont.)

I. INTRODUCTION

Miniaturized capacitors with high dielectric constants (K), low dissipation factors, stable voltage and temperature characteristics are required in modern electronic devices. Two principal types of capacitors have been developed: (i) thin capacitors with high permittivities and, (ii) monolithic capacitors with many internal dielectric layers connected in parallel. However, despite the realization of high dielectric constants up to 10,000, thin film capacitors have suffered from defects and reliability problems and, monolithic capacitors from practical thickness limitations.

Internal boundary layer capacitors (IBLC) have been developed recently, with dielectric constants over 50,000, and surprisingly stable temperature and voltage characteristics; with low dissipation factors less than 1%. However, the nature of ceramic microstructure and its relationship to electrical properties is not well understood. It is hypothesized that internal boundary layer capacitors are comprised of an array of semiconducting grains, surrounded by thin insulating boundaries. n-type semiconductivity in perovskite ceramics can be achieved by a variety of mechanisms including: (i) controlled valence doping by aliovalent ions (which are of the correct ionic size to substitute in the lattice), or by (ii) sintering in a reducing atmosphere. Insulating internal boundary layers can be reintroduced

by: (i) chemical counterdoping or (ii) gaseous reoxidation along grain or phase boundaries. Conceptually, internal boundary layer dielectrics can be thought of as an heterogeneous distribution of resistivities between conducting grains (n-type) and insulating boundaries. The resistivity distribution can be approximated by a series microstructure model, where continuously connected boundaries normal to flux passage block the transport of charge, thus setting up thin interfacial space charge layers of subsequent high capacitance and apparent dielectric constant ($\bar{K}'$).

An attempt was made to gain knowledge of individual grain and boundary conditions, with investigations on microstructure and microscale electrical measurements, so as to determine their intrinsic properties. A model was subsequently proposed to explain extrinsic polycrystalline properties in terms of intrinsic single grain and boundary characteristics.

Fine grain microstructures, suitable for multilayer internal boundary layer capacitors, were developed by microstructural engineering techniques. Semiconducting $SrTiO_3$ grain boundaries were reinsulated by liquid phase sintering with $Pb_5Ge_3O_{11}$ and B_2O_3. These materials were chosen because they melt at relatively lower temperatures, solidify to insulators, and are grain growth inhibitors.[1]

II. LITERATURE REVIEW

Since anomalously high apparent dielectric constants ($\bar{K}'$) were first reported for certain types of polycrystalline ceramic materials,[2] much work[3-7] has been done on semiconducting ceramics for the development of high capacitive devices. n-type semiconductivity in the perovskite family of materials can be achieved by either sintering in a reducing atmosphere or,by aliovalent doping. Donor ions incorporated at Ba^{2+} sites carry an excess positive charge, which may be compensated by either (i) the formation of conduction electrons, (which is favored at low oxygen partial pressures and high temperatures) or by (ii) cation vacancies (which predominate at low temperatures and high oxygen partial pressures[8]). Analogous monovalent substitution results in p-type semiconductivity which is observed only at elevated temperature due to deep traps, or at high oxygen partial pressures due to acceptor-type vacancies in the barium sublattice.[9] (It is even reported that anomalous n-type semiconductivity can be obtained at room temperature in $BaTiO_3$, which contains small amounts of Ag^+ substituted for Ba^{2+}.[10])

For explanations of semiconducting behavior in doped $BaTiO_3$, Saburi[11] proposed a hopping model, whereas Gerthsen et al[12] have proposed a polaron model. Daniel et al[8] have reported that n-type semiconductivity is increased with dopant concentration up to a certain limit, and for higher dopant concentrations, the conductivity decreased anomalously as shown in Figure

1. This phenomenon was explained in terms of acceptor traps compensating for donors. For the case of La_2O_3 doped $BaTiO_3$, two neighboring Ba^{2+} ions may be replaced by two La^{3+} ions,[11] for example, with the barium vacancy coupled to this pair, thus forming an acceptor trap.[13]

The electrical conductivity of polycrystalline ceramics made semiconducting by aliovalent doping is extremely sensitive to the concentration and distribution of dopants and sintering conditions. Several workers investigated the effect of dopants on the semiconductivity and microstructure of $BaTiO_3$. Ueoka[14] reported 0.1-0.6 atomic % doping with transition elements was effective, though the optimum concentration differed from additive to additive. For the case of rare-earth dopants,[15] the electrical conductivity increased with increasing dopant concentration at low levels, but exhibited a maximum conductivity at a specific dopant content. Large grain sizes (> 10 μm) resulted when the dopant concentration was less than 0.2 atomic %, and the lattice constants were similar to the undoped material. Grain growth was inhibited by doping at higher levels, and the lattice constants changed. Conductivities less than 10 Ω^{-1}-cm^{-1} were obtained for addition of Al_2O_3, SiO_2 and TiO_2 to $BaTiO_3$, which was sintered in the 1280-1380°C temperature range.[16] Kahn[17] reported higher electrical conductivities in larger grain microstructures for niobium doped $BaTiO_3$. Saburi[11] reported in a study of 0.1 mole % Ce doped $BaTiO_3$, that compositions greatly different from pure $BaTiO_3$, did not yield readily to valence doping techniques.

Intergranular blocking layers were important for many electrical properties in semiconducting-insulating electrical

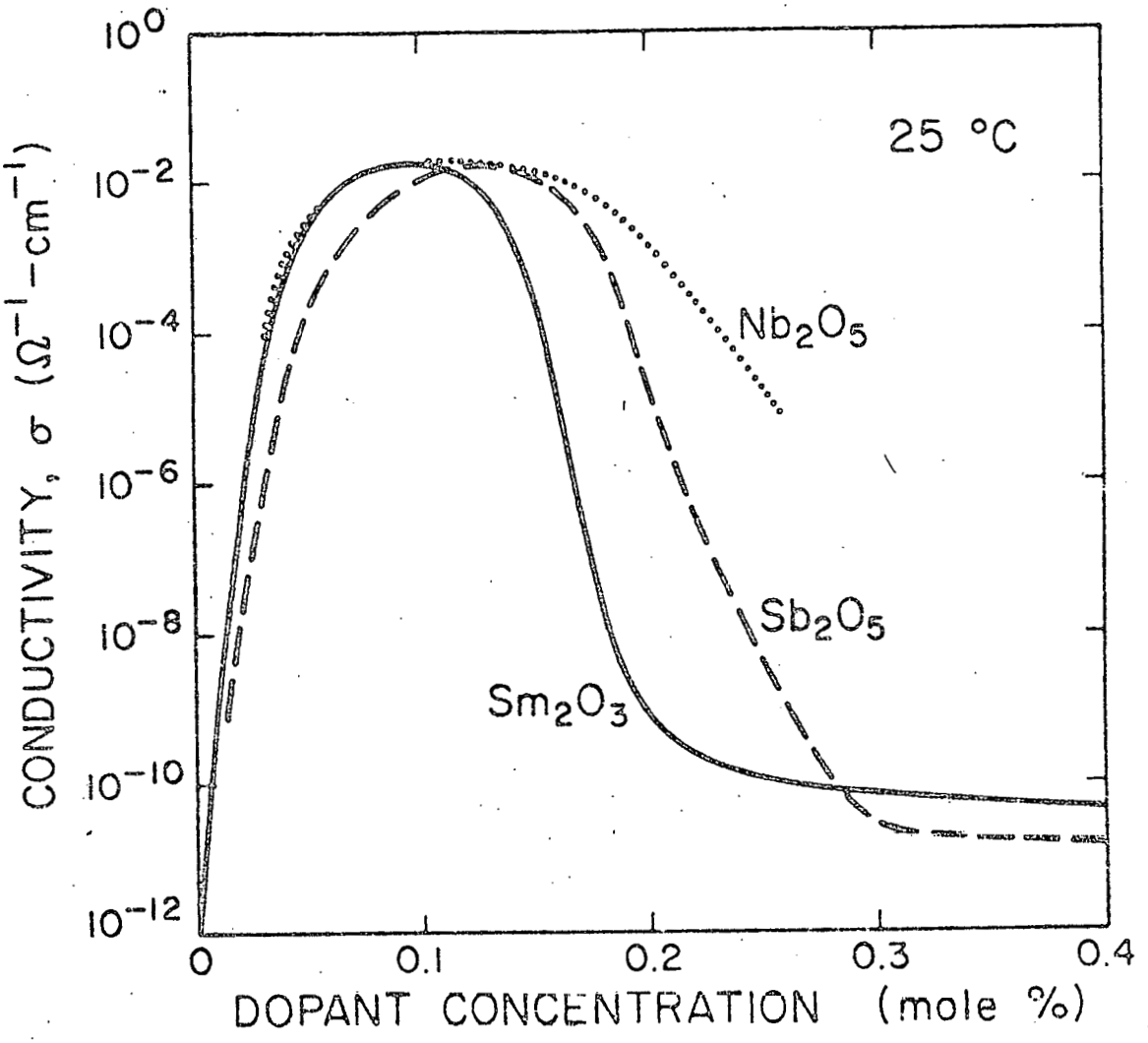

FIGURE 1. Conductivity vs. Doping Concentration for Polycrystalline $BaTiO_3$.

ceramics. For $BaTiO_3$, an increasing thickness of blocking layer leads to a continuous change from PTC resistor characteristics, to internal boundary layer capacitor behavior. Heywang[13,18-20], in a pioneering series of papers, discussed the electrical behavior of semiconducting $BaTiO_3$ in terms of potential barriers (i.e., depletion layers). These could form at the surface of $BaTiO_3$ grains due to acceptor-type surface states, but the nature and formation of these surface states have not yet been satisfactorally explained. Heywang[13] proposed the potential barriers formed due to preferential segregation of acceptor cations at the internal surfaces or grain boundaries, whereas Jonker[21] attributed the surface states to anion adsorption at grain boundaries. Daniel et al[22] considered the surface states as thin diffusion layers, with an increased concentration of barium vacancies at the grain boundaries. Recently, Wernicke[23] proposed a two layer model (diffusion layer and second phase layer) to explain the dielectric behavior of IBL capacitors based on $SrTiO_3$. Insulating boundary layers were introduced in a second firing, in which a $PbO-Bi_2O_3-B_2O_3$ mixture was infiltrated at 1000-1200°C in air.[24] Vojnovich[25] suggested the formation of insulating barriers on reduced $BaTiO_3$ was a diffusion controlled process, in which anion diffusion occurred into the oxygen deficient lattice. Thus, capacitance and resistance characteristics of internal barrier layer capacitors might be greatly influenced by reoxidation processes.

Several studies have also been carried out on the interrelationships between microstructure and electrical properties, so as to determine the nature of interfacial states. Barrier

layers were made visible by decoration techniques[12], and by ion induced electron emission microscopy.[26] Microprobe investigations showed acceptor dopants were concentrated mainly in the interface region,[13] which were high resistance regions, as determined by measurements of potential profiles with a travelling probe. Gerthsen et al[27] measured single grain boundary capacitance by a slicing and thinning technique, and suggested that an intermediate layer of the rich second phase might exist at grain boundaries, between neighboring $BaTiO_3$ grains. Wernicke,[24] in the study of $PbO-Bi_2O_3-B_2O_3$ infiltrated semiconducting $SrTiO_3$, explained the formation of a second phase in terms of selective melting reactions; and the composition of the second phase layer was proposed to be a layered perovskite type material (probably $Pb_2Bi_4Ti_5O_{18}$), which recrystallized from a glassy matrix. Bongers et al[28] studied the microstructures of IBL capacitor based on $SrTiO_3$, in which Bi_2O_3, PbO and B_2O_3 were also infiltrated into reduced $SrTiO_3$ discs and reported that $SrTiO_3$ grains appeared to be completely surrounded by a second phase, which was identified by x-ray diffraction and electron microscope lattice fringe imaging techniques, but was identified this time as crystalline $Sr_2Bi_4Ti_5O_{18}$. The thickness of the secondary phase was estimated from SEM micrographs to be of the order of 0.1 to 0.5 μm.

Most of the fabrication processes for IBL capacitors are reported in the patent literature. Dielectric constants of 75,000 were obtained in the system[29] $(Ba_{1-x}M_x^{2+})O \cdot Z(Ti_{1-y}M_y^{4+})O_3$, where M^{2+} represents Ca, Sr, Pb or Mg and M^{4+} was Zr, Sn; and Z had values between 1.005 to 1.05. This formulation contained at least two different dopants, of which one (e.g., Sb, La, Nb, Bi)

produced n-type semiconductivity in the grains, and the other (e.g., Cu, Fe, Mn) compensated for n-type conductivity at the surface layers. IBL capacitors with a dielectric constant of 40,000 were also developed using pure $SrTiO_3$.[30] Nb_2O_5 or Ta_2O_3 were used as donor dopants; and Bi_2O_3 (or mixtures of Bi_2O_3 with PbO and B_2O_3) was diffused in for formation of insulating boundary layers. IBL capacitors based on paraelectric $SrTiO_3$ had improved temperature stability; and were more suitable for high frequency applications, than IBL capacitors based on $BaTiO_3$.[31]

Formation of insulating boundary layers is dependent on the type of dopants and their amount, and the second firing process. Waku[32] reported in his study on Dy_2O_3 doped $BaTiO_3$, that Cu, Mn, Bi and Tl were the most desirable counter dopants for high dielectric constants, and low dissipation factors, in a relatively wide concentration range. Dielectric constants and dissipation factors decreased, and resistivity increased rapidly, with increasing second firing temperatures. The dielectric characteristics were affected by the BaO/TiO_2 stoichiometry ratio of the starting materials. The most desirable values were between 1.01-1.02.

Anomalous electrical behavior of heterogeneous dielectrics may be explained in terms of Maxwell-Wagner theory. Maxwell[33] theoretically demonstrated the possibility of dielectric absorption in double layer dielectrics, where constituent layers had differing electrical conductivities. Wagner[34] derived expressions for the dielectric constant and dielectric loss, of mixtures containing conducting spheres dispersed within a uniformly insulating dielectric continuum.

When a composite material's dielectric behavior differs from either the constituent materials, due to space-charge polarization processes, this effect has been termed Maxwell-Wagner behavior. Several methods were proposed to analyse dielectric dispersion data. Cole-Cole analysis[35] has been known to be an effective method for representing dielectric dispersion behavior, in which the dielectric constant $K'(\omega)$ is plotted against dielectric loss $K''(\omega)$ in the complex plane. Materials possessing ideal Debye-type relaxation behavior can be described by the following set of equations:

$$K' = K'_{\infty} + \frac{K'_S - K'_{\infty}}{1 + \omega^2\tau^2} \tag{1}$$

$$K'' = \frac{(K'_S - K'_{\infty})\omega\tau}{1 + \omega^2\tau^2} \tag{2}$$

where

K'_S is the static dielectric constant

K'_{∞} is the high frequency dielectric constant

K'' is the dielectric loss

ω is $2\pi \cdot$ frequency

τ is the relaxation time.

The Cole-Cole relationship would be represented by a semicircle, with its center on the $K'(\omega)$ axis, and intercepts corresponding to K'_S and K'_{∞}. However, this single-type relaxation behavior is rarely observed in complex ceramic materials. Generally, what is observed, is a broader range for dielectric constant relaxation and

dielectric loss, absorption, accompanied by smaller maximum values of dielectric loss, than predicted by the simple Debye theory, as illustrated in Figure 2. K. S. Cole and R. H. Cole[35] suggested that for this more complex situation, the dielectric behavior might follow an empirical expression,

$$K^* = K'_\infty + \frac{K'_s - K'_\infty}{1 + (j\omega\tau)^{1-\alpha}} \quad , \tag{3}$$

where K* was the complex dielectric constant, j, the imaginary number, and α, a distribution coefficient between 0 and 1. Cole and Davidson[37] found that experimental results for certain materials did not exhibit symmetrical relaxation arcs, but a skewed distribution. This was represented by

$$K^* = K' + \frac{K'_s - K'}{(1 + j\omega\tau)^{\alpha}} \tag{4}$$

with a distribution constant α between 0 and 1.

The Maxwell-Wagner model of a diphasic dielectric has been successfully applied by several investigators to explain the dispersion behavior of semi-insulating ceramic materials. Electrical parameters for a diphasic series microstructure were derived by Hilborn[38] and presented later by Payne.[39] Koops[5] explained the dielectric relaxation behavior of nickel-zinc ferrite by assuming semiconducting grains were surrounded by insulating layers. Dielectric dispersion behavior of ZnO varistors (the microstructures of which consist of semiconducting ZnO grains and insulating boundary layers) was explained in terms of a Maxwell-Wagner model.[40]

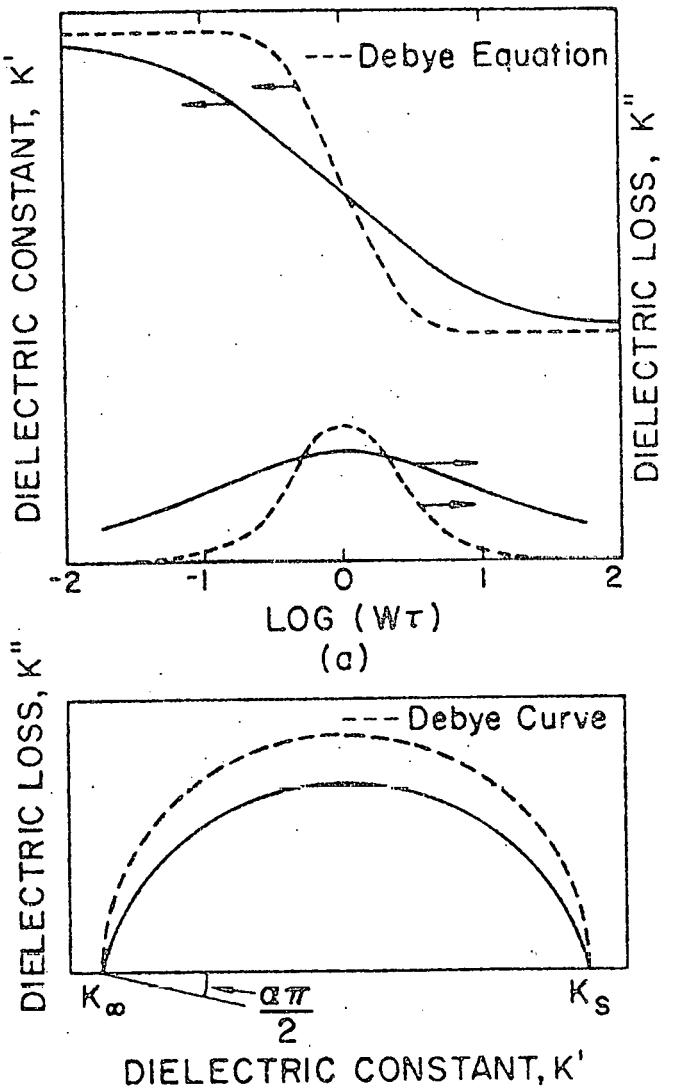

FIGURE 2. Dielectric Dispersion Behavior.[35]

Hilborn[38] studied dielectric dispersion in sintered compacts of α-Fe_2O_3, and analysed the data in terms of a multiple-layer model which was analogous to that described by Cole and Davidson.

Turik et al[41] studied the dielectric dispersion behavior of polycrystalline ferroelectrics of the perovskite structure, over a broad frequency range, and reported a relaxation frequency around 100 MHz for chemically pure $BaTiO_3$. Coarse grain material (50 μm) had a lower distribution factor (α = 0.03) than fine grain material and a near semicircular arc; whereas fine grain $BaTiO_3$ (1 μm) showed a high distribution factor (α = 0.41), deviating markedly from simple Debye behavior when analyzed on a Cole-Cole plot. For semiconducting $(Ba,Sr)TiO_3$ solid solutions, the relaxation frequency increased with increasing Sr content, into the gigahertz region for $Ba_{0.5}Sr_{0.5}TiO_3$. Similar results were reported for $BaTiO_3$ and $(Ba,Sr)TiO_3$ IBL capacitors.[42] Edahiro et al.[31] explained dielectric dispersion behavior of IBL capacitors based on $SrTiO_3$ by Maxwell-Wagner theory; and reported the relaxation frequency, which was around 10^5Hz, shifted to lower frequencies as the conductivity of the grains decreased, which was to be expected from Maxwell-Wagner theory. The relaxation frequency was found to increase with increasing ionic size of the aliovalent rare-earth ions (Re) substituted into the $SrTiO_3$-$ReFeO_3$ based capacitors.

III. PROPOSED MODEL

The dielectric properties of polycrystalline internal boundary layer capacitors (IBLC) are greatly influenced by the electrical boundary conditions existing at grain and phase boundaries. Two extremes of ceramic microstructures have been proposed,[43] which in turn, depend upon the ceramic processing conditions used, and which may be engineered into ceramics for the development of specific properties: (i) grain/grain separation by an insulating boundary phase (i.e., a proposed n-i-n structure), and (ii) grain/grain contact with intermediate surface state (i.e., a proposed n-c-n structure).

On the basis of microstructural analysis and microscale electrical measurements, commercial internal boundary layer (IBL) capacitors were found to often exhibit an hybrid representation between these two end member assemblages (i.e., a n-c-i-c-n structure).

A. n-i-n Structure

The microstructure of research and development IBL capacitors, in which the boundaries between n-type semiconducting grains were reinsulated by liquid phase sintering techniques (with $Pb_5Ge_3O_{11}$ or B_2O_3), can be represented by a diphasic structure, in which cubes of uniformly low resistivity grains were completely surrounded by a continuously connected insulating boundary region.

B. n-c-i-c-n Structure

For commercial IBL capacitors formed from $BaTiO_3$ and $SrTiO_3$ by valence doping, chemical counterdiffusion and reinsulation methods, the microstructure can be expressed in terms of a triphasic structure, in which an intermediate layer forms in the subsurface of semiconducting grains by limited diffusion or segregation, in addition to insulating boundaries between the grains. The intermediate compensation layer can be thought of as a Schottky type depletion layer, in which the capacitance would be dependent upon applied voltage.

Since the boundaries are continuously connected as illustrated in Figure 3, the microstructure of IBL capacitors can be approximated by a brick-wall model of ceramic microstructure, which facilitates analysis of electrical properties. Series mixing rules are appropriate for heterophasic IBL capacitors in which the resistive boundaries normal to flux passage interrupt the lines of flux, i.e., resistivity distribution by the boundary conditions.[39] Furthermore, the brick-wall model can be reduced to a Maxwell-Wagner multilayer model, since the total impedence of a set of series connected impedences (representing dielectric layers arranged at random in plane strata normal to the electric displacement) is independent of their sequence.

An energy band diagram at thermal equilibrium and a corresponding electrical equivalent circuit for a 3-layer model, is shown in Figure 4, where each layer has capacitance paralleled by resistance. The apparent junction capacitance ($\bar{C}$) per unit area, is given by the capacitance of the insulating layer (C_i) and the series connected forward (C_c^F) and reverse (C_c^R) biased layers,

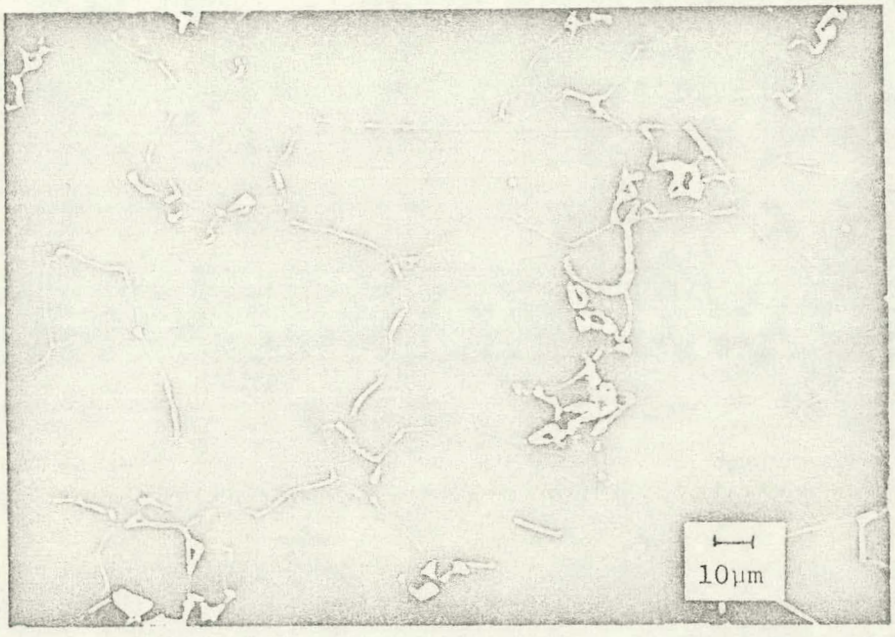

FIGURE 3. SEM photomicrograph of a polished surface of an IBL capacitor based on $SrTiO_3$ in the backscattered electron mode.

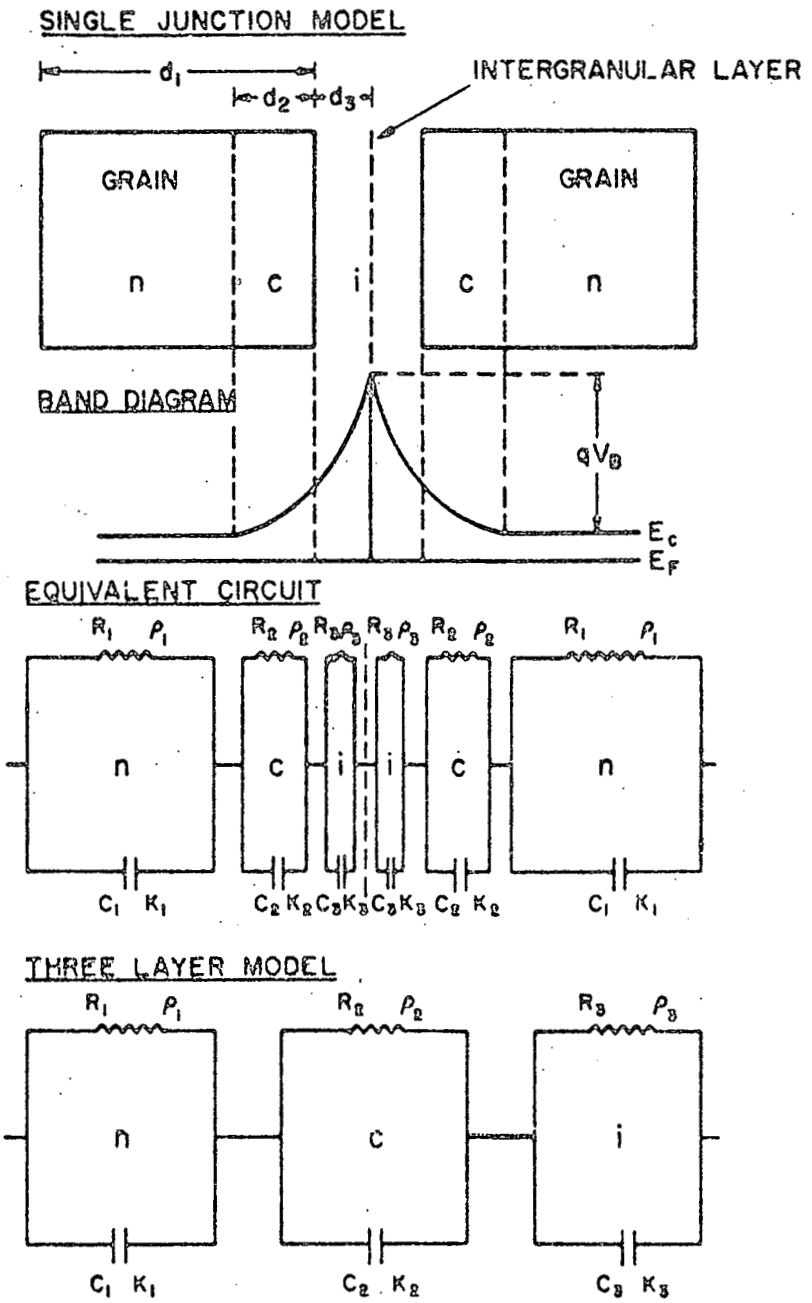

FIGURE 4. Energy band diagram and equivalent n-c-i-c-n representation of barrier characteristics for an IBL capacitor.

i.e.,

$$\frac{1}{\bar{C}} = \frac{1}{C_i} + \frac{1}{C_c^F} + \frac{1}{C_c^R} \tag{5}$$

which is equivalent to

$$\frac{1}{\bar{C}} = \frac{2d_3}{\varepsilon_0 K_3} + \left[\frac{2(V_B - V)}{qN_D^+ \varepsilon_0 K_2}\right]^{\frac{1}{2}} + \left[\frac{2(V_B + V)}{qN_D^+ \varepsilon_0 K_2}\right]^{\frac{1}{2}} \tag{6}$$

where, ε_0 is the permittivity of free space, K_3 and K_2 the respective dielectric constants of the insulating and intermediate layers, q the elcctronic charge, and N_D^+ the concentration of uncompensated ionized donors.

In a system within layers, in which the electrical properties are dissimilar, the electrical parameters of the overall composite can be expressed by the following equation,[44]

$$\bar{K} = \frac{\sum_{i=1}^{n} d_i \sum_{i=1}^{n} \frac{d_i}{K_i} \cdot \frac{\tau_i^2}{1 + \omega^2 \tau_i^2}}{\left[\frac{d_i}{K_i} \cdot \frac{\tau_i}{1 + \omega^2 \tau_i^2}\right]^2 + \left[\sum_{i=1}^{n} \frac{d_i}{K_i} \cdot \frac{\omega \tau_i^2}{1 + \omega^2 \tau_i^2}\right]^2} \tag{7}$$

where $\tau_i = \varepsilon_0 K_i \rho_i$, ρ_i is the resistivity and d_i, the thickness of the layer. For the simplest case, where n = 2, the material properties may be expressed by the following set of equations:

$$\bar{K}_s' = d\left[\frac{\rho_1^2 K_1' d_1 + \rho_2^2 K_2' d_2}{(\rho_1 d_1 + \rho_2 d_2)^2}\right] \tag{8}$$

$$\bar{K}_{\infty}' = \frac{K_1' K_2' d}{K_1' d_2 + K_2' d_1} \tag{9}$$

$$\bar{K}' = K_{\infty}' + \frac{\bar{K}_s' - \bar{K}_{\infty}'}{1 + \omega^2 \tau_k^2} \tag{10}$$

$$\tau_k = \frac{\varepsilon_0 \rho_1 \rho_2 (\bar{K}_1' d_2 + \bar{K}_2' d_1)}{\rho_1 d_2 + \rho_2 d_1} \tag{11}$$

where $\bar{K}_1'$ is the static dielectric constant, $\bar{K}_{\infty}'$, the dielectric constant at high frequency and τ_k, the relaxation time. Application of Equation 7 to a 3-layer structure, which is given in Appendix C, was too complex and impractical for a rigorous analysis of the dispersion behavior of IBL capacitors. A more simple and efficient method was proposed to represent the dielectric dispersion behavior of IBL capacitors. The two-layer Maxwell-Wagner theory was applied for each of the adjacent two layers, i.e., one for the insulating/intermediate interface, the other for the semiconducting grain/intermediate layer interface. Material properties can now be estimated from the following set of equations:

$$\bar{K}_{s,nc}' = d\left[\frac{\rho_1^2 K_1' d_1 + \rho_2^2 K_2' d_2}{(\rho_1 d_1 + \rho_2 d_2)^2}\right] \tag{12}$$

$$\bar{K}_{\infty,nc}' = \frac{K_1' K_2' d}{K_1' d_2 + K_2' d_1} \tag{13}$$

$$\bar{K}_{nc}' = \bar{K}_{\infty,nc}' + \frac{\bar{K}_{s,nc}' - \bar{K}_{\infty,nc}'}{1 + \omega^2 \tau_{k,nc}^2} \tag{14}$$

$$\tau_{k,nc} = \frac{\varepsilon_0 \rho_1 \rho_2 (K_1'd_2 + K_2'd_1)}{\rho_1 d_2 + \rho_2 d_1} \tag{15}$$

$$\bar{K}'_{s,ci} = d\left[\frac{\rho_2^2 K_2' d_2 + \rho_3^2 K_3' d_3}{(\rho_2 d_2 + \rho_3 d_3)^2}\right] \tag{16}$$

$$\bar{K}_{\infty,ci} = \frac{K_2' K_3' d}{K_2' d_3 + K_3' d_2} \tag{17}$$

$$\bar{K}'_{ci} = \bar{K}'_{\infty} + \frac{\bar{K}'_{sci} - \bar{K}'_{\infty ci}}{1 + \omega^2 \tau_{k,ci}^2} \tag{18}$$

$$\tau_{k,ci} = \frac{\varepsilon_0 \rho_2 \rho_3 (K_2' d_3 + K_3' d_2)}{\rho_2 d_3 + \rho_3 d_2} \tag{19}$$

where subscripts nc,ci refer to semiconducting/compensation interface and compensation/insulating interface, respectively. Current-voltage characteristic, capacitance-voltage characteristic and dielectric dispersion behavior of IBL capacitors may be interpreted in terms of this proposed 3-layer model. Calculated values of $\bar{C}(V)$, K_s', K_∞', τ_k will be later shown to be in good agreement with experimental data. These parameters are listed in table 3.

IV. EXPERIMENTAL PROCEDURE

A. Specimen Preparation

Internal boundary layer capacitors used in this study were representative of the types of units currently manufactured from $BaTiO_3$ and $SrTiO_3$. In addition, research and development IBL capacitors, with different microstructures than commercial units, were prepared in our laboratory from $SrTiO_3$. Reagent grade strontium titanate powder (218-2) was obtained from the Transelco Division of Ferro Corporation. The powder was doped with 2 wt.% WO_3 and calcined in a reducing atmosphere. Mixing and milling of carefully weighed proportions were carried out in plastic jars containing ZrO_2 media and deionized water. A mixing of 3 hours was used. After drying, the powders were gaseously reduced in an externally wound (Pt) tube furnace at 1380°C for 3 hours. A flow of forming gas (90% N_2 + 10% H_2) was introduced after one hour at peak temperature, and terminated after cooling below 1100°C. Pt/Pt-10% Rh thermocouples were used in conjunction with digital temperature indicators. When forming gas was used, the thermocouples were placed outside the tube, so as to prevent hydrogen embrittlement. Black semiconducting $SrTiO_3$ calcined powder was crushed and mixed with 10 wt.% reagent grade $Pb_5Ge_3O_{11}$ or 10 wt.% B_2O_3 and milled for 3 hours in plastic jars. After drying, the powders were granulated with 5% PVA aqueous solution and pressed into 1.2 cm in diameter by 0.1 cm thick discs, which were fired

on ZrO_2 setters at 1000°C for 2 hours in air. Electrode terminations were made with a Dupont 6730 type silver fritted ink, which was fired on in air at 750-800°C for 20 minutes. IBL capacitors investigated in this thesis are designated in Table 1.

B. Microstructure Analysis

Elemental analyses of IBL capacitors were carried out by mass spectrographic techniques. Polished and thermally etched specimens were examined with a JEOL U3 or JEOL JSM-35C scanning electron microscope (SEM). Surfaces were polished after epoxy mounting on aluminum stubs, and ground with 15, 3, 1, 0.1 μm diamond pastes. Thermal etching was carried out by heat treatments at 1150°C for 30 minutes. Specimens could be examined on a SEM without having evaporated conducting coatings deposited, but the best images were obtained when a thin film of carbon was deposited. To determine the compositional difference between grains and grain boundary regions, the specimens were also examined in a SEM using backscattered electron imaging, where the number of backscattered electrons was proportional to the atomic number of the element present. The chemical composition of grain boundary regions were also examined with a JEOL JXA-50A scanning electron microprobe (EPMA), in conjunction with a wavelength dispersive spectrometer (WDS). Specimens were prepared for scanning transmission electron microscopy analysis (JEOL 200 kV STEM) by (i) either a two-step replica method or by (ii) ion-thinning techniques. For carbon replicas (i) a few drops of 4% solution of collodian amyl acetate were placed on a polished surface, and after drying, the film was removed, shadowed by Cr

TABLE 1

IBL Capacitors Investigated

Designation	Major Material	Proposed Structure	Source
G	$BaTiO_3$	n-c-i-c-n	commercial
J-1	$SrTiO_3$	n-c-i-c-n	commercial
J-2	$SrTiO_3$	n-c-i-c-n	commercial
I-1	$SrTiO_3$-$Pb_5Ge_3O_{11}$	n-i-n	development
I-2	$SrTiO_3$-B_2O_3	n-i-n	development
K-1	$SrTiO_3$-Cu_2O	n-c-i-c-n	development

evaporation (for improved contrast) and a carbon film was later deposited. Molten microcrystalline wax was poured over the carbon replica, and the amyl acetate film dissolved away in acetone. The wax was finally dissolved in xylene. For the ion-milling (ii), thin slices were cut on a diamond wafering blade, polished to less than 30 μm thick, and finally thinned on an ion miller (Technics Model IV). Wedge-shaped specimens were obtained. Ion milling was carried out at an oblique angle of incidence (~ 15°), with Ar ions accelerated to 4 kV, to restrict induced radiation damage to the upper and lower surfaces of the wedge. The ceramic microstructure was examined on a STEM (JEOL 200 kV). Energy dispersive x-ray analysis (XED) with a spatial resolution of less than 50 Å could be obtained under favorable circumstances. Dedicated microstructural analysis, chemical location of segregated and intergranular layers, and diffusion profiles of grain interfaces,were determined with an HB5 STEM, equipped with a field emission gun, and which operated in an energy dispersive X-ray microanalysis mode. The current model uses a field emission gun as an electron source,which results in a fine probe size (5 Å). Contamination of the specimen during analysis was prevented by the high vacuum pressure (10^{-9} torr). Point to point compositional analysis was carried on with a linear spacing of 100 Å (i.e., probe center to probe center).

C. Electrical Measurements

D.C. resistance was measured with a Keithly 610C electrometer. The specimen was placed between two electrodes in a chamber which was placed in a tube furnace. Current-voltage characteristics were measured with a Keithly electrometer and a d.c. power

supply, in a current range up to 100 mA. Voltage dependent capacitance and dissipation factors were measured with a Hewlett Packard 4270A automatic capacitance bridge in the d.c. voltage range between 0 and 200 volt. Frequency dependent measurements were made at 0.01 Vrms with the Hewlett Packard bridge in the medium frequency range (1 KHz - 1 MHz), and with a RF admittance bridge (Boonton electronics 33A/1) at high frequencies (1 MHz - 100 MHz). The dissipation factor was calculated from conductance data using the following expression,

$$D = \frac{G}{\omega C} \tag{20}$$

where G was the conductance in mhos, ω, $2\pi \cdot$ frequency, and C, the capacitance in farads. Adjusted values of dielectric loss, in which the d.c. conductivity (σ) was subtracted from the a.c. conductance, are given in Figures 28-30. These data were calculated from,

$$K'' = (K_s - K_\infty) \frac{\omega\tau}{1 + \omega^2\tau^2} + \frac{\sigma}{\varepsilon_0\omega} \tag{21}$$

Microscale electrical measurements were carried out on polished but unetched surfaces of specimens, over which a checkerboard pattern of electrode pads had been deposited by Pd/Au evaporation through a fine grid network of silver mesh. Specimens were epoxy mounted on 0.2 mm thick Al_2O_3 substrates and placed on the stage of an optical microscope (Leitz Ortholux). Contacts were made to the electrode pads (25 x 25 μm) by tungsten wire probes (10 μm tips), which were positioned by micromanipulators

under the compound microscope, as illustrated in Figures 5 and 6. Measurements at magnifications greater than 200x were difficult to carry out because of the short working distance. The microscope was fitted with a warm stage, so that the temperature dependence of $\bar{K}'$ and $\bar{\rho}$ could be determined for individual grains and boundary regions, by preselecting appropriate electrode pads. The electrical resistivities of grains were calculated from sheet resistances by

$$\rho_G = R_s \cdot X_j \tag{22}$$

where R_s was the measured sheet resistance and X_j, the depth, which was taken to be equivalent to the grain diameter. Resistivities of grain boundary regions were calculated from

$$\rho_{GB} = R \frac{A}{d} \tag{23}$$

where R was the measured resistance, A, the area (assumed to be the grain diameter for near cubic grains) and d, the thickness of the boundary region. The dielectric breakdown voltage for a junction was measured at constant current (5 mA). Over 20 junctions were measured and analyzed. Temperature dependent measurements were made with the aid of a chromel-alumel thermocouple. Above 150°C, thermal expansion difficulties caused the probe tips to move off their original contact points. Measured values of the electrical characteristics of single junctions varied somewhat from junction to junction, and so measurements were made of at least 20 separate junctions. Typical but average values were used in the analysis of electrical properties of single junctions.

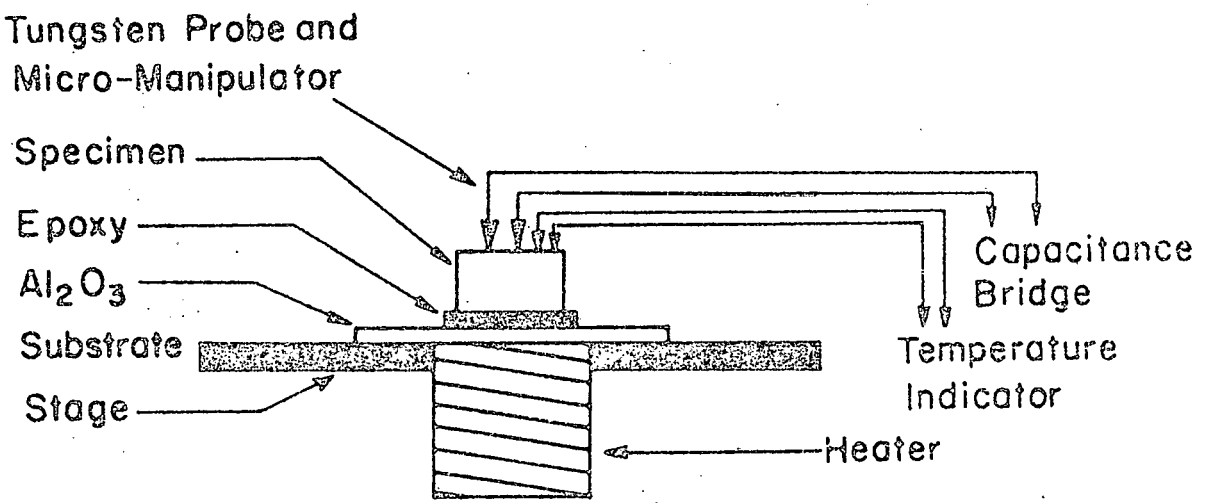

FIGURE 5. Microscale electrical measurement assembly.

FIGURE 6. Optical photomicrograph of microscale electrical measurements across a boundary region.

V. RESULTS AND OBSERVATIONS

A. Microstructure Analysis

Elemental analyses of IBL capacitors, determined by mass spectrographic techniques, are listed in Table 2. For IBL capacitors based upon $BaTiO_3$, the compositions contained essentially minor additions of Sn and Sr. Elemental distributions were determined further by dispersive x-ray analysis. Figure 7 illustrates a typical microstructure of a polished and thermally etched surface of a type G IBL capacitor based on $BaTiO_3$. The grain size ranged between 20-50 μm, with an intergranular phase of anisotropic crystalline morphology. Electron probe microanalysis (EPMA) identified the grains to be $(Ba,Sr)(Ti,Sn)O_3$, and the boundary phase to be titania rich. Ti $K\alpha_{1,2}$:Ba $L\alpha_1$ was 1:1 in the grains but 1.64:1 in the grain boundaries, as illustrated in Figure 8. Silica was also found to be preferentially concentrated within the boundary phase, with alumina only being present in the boundary region.

A scanning photomicrograph of a polished surface of a J-1 type IBL capacitor based on $SrTiO_3$, determined in the backscattered mode, was previously presented in Figure 3. The average grain size was 30 μm, and the bright boundary region was approximately 1 μm thick. The continuous bright boundary phase indicates high atomic number elements were concentrated in the boundary region. A transmission photomicrograph of a replica of a polished and thermally etched surface of this capacitor is given in Figure 9,

TABLE 2

Semiquantitative Analysis of IBL Capacitors

	IBL Capacitor G	IBL Capacitor J-1
Major (> 1.0%)	Ba, Ti, Sr, Sn	Sr, Ti
Minor (> 0.1%)	Si, Mg, Na, Zn, Ni, Fe, P	Si, Na, Al, Mg, Ba, Ca
Trace (< 0.1%)	Ge, V, Ca, Cl, Al, Cu, Cr, F, W, B, Ta, Nb, La, Zr, Be, K	Bi, Pb, Mo, Nb, Zr, Zn, Ni, Cl, S, Ta, Te, Co

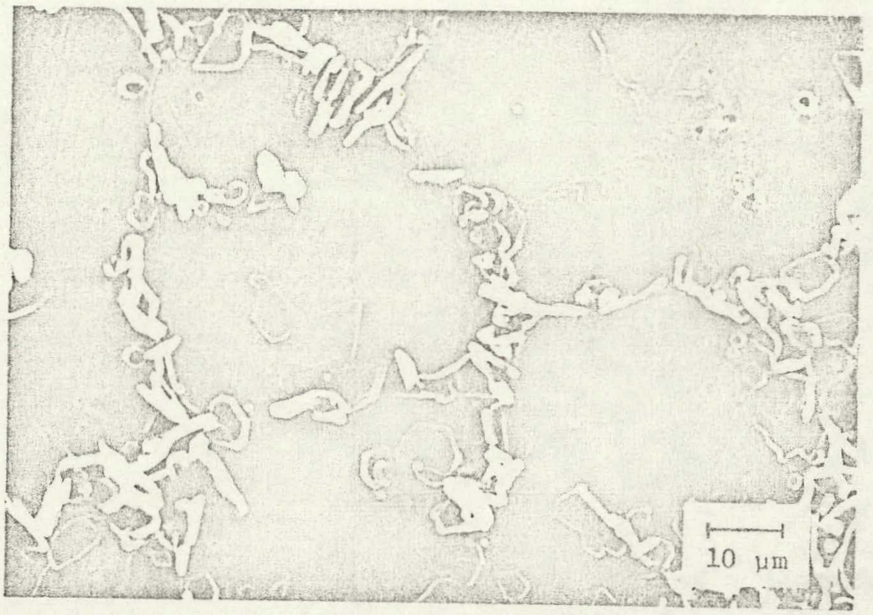

FIGURE 7. SEM photomicrograph of a polished and thermally etched surface of an IBL capacitor based upon $BaTiO_3$.

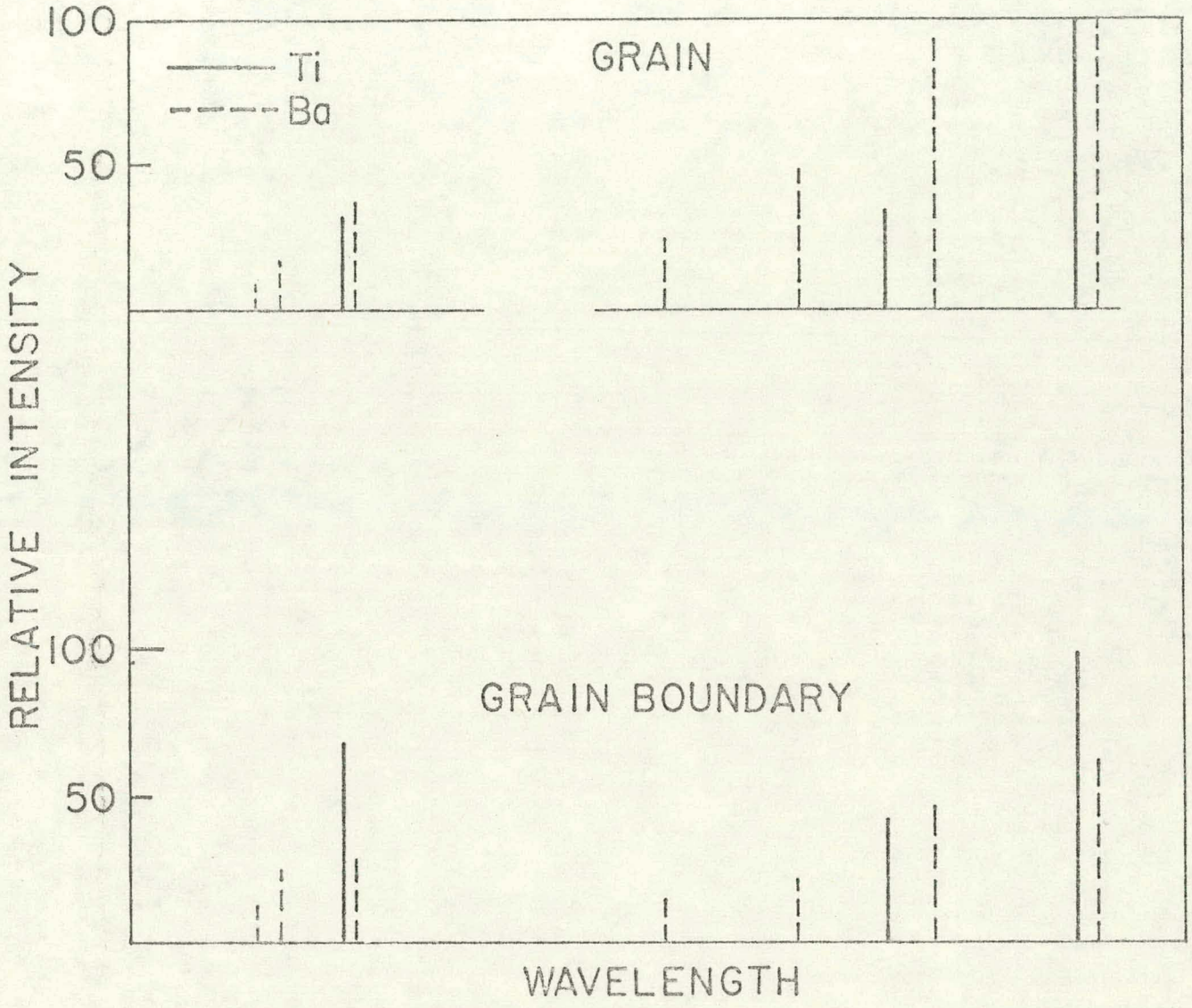

Figure 8. X-ray wavelength dispersive spectroscopy for an internal boundary layer capacitor based on $BaTiO_3$

and illustrates the presence of an intergranular layer with morphology different from that of the grain. (The boundary appears unusually wide in this photomicrograph due to thermal grooving.) Electron diffraction patterns and TEM photomicrographs of an ion milled specimen, of the same capacitor, are illustrated in Figure 10. Thin intergranular layers, which have different crystalline structure, are clearly evident from the photomicrograph. The thickness of the intergranular layer is about 0.1 μm. High Bi concentration in the intergranular layer was determined by x-ray energy dispersive analysis, as illustrated in Figure 11. Bi was not detected in the grains.

Compositional STEM analyses for polished but unetched surfaces, in which the intergranular boundary thickness was 0.3 μm, are given in Figure 12. The data indicate Bi was preferentially concentrated in the boundary region. Integrated intensities as a function of distance, illustrate the concentration profile for Bi; which was concentrated in a 300 Å wide boundary region, and extended 100 Å into the sub-surface of the grain. Data for research and development IBL capacitors are given in Figures 13 and 15. Figure 13 illustrates the microstructure for a capacitor formed from $SrTiO_3$ powder, which was doped with WO_3, and which was fired in a reducing atmosphere. A Cu_2O counterdopant was later diffused in from the external surfaces by a second firing treatment at 1100°C in air for 2 hours. Figure 13 illustrates the presence of an intergranular layer, which was identified by x-ray dispersive analysis to contain Cu (Figure 14). The crystalline nature of this layer was identified by electron

FIGURE 9. TEM photomicrograph of a polished and thermally etched section of an IBL capacitor based upon $SrTiO_3$ prepared by the replica method.

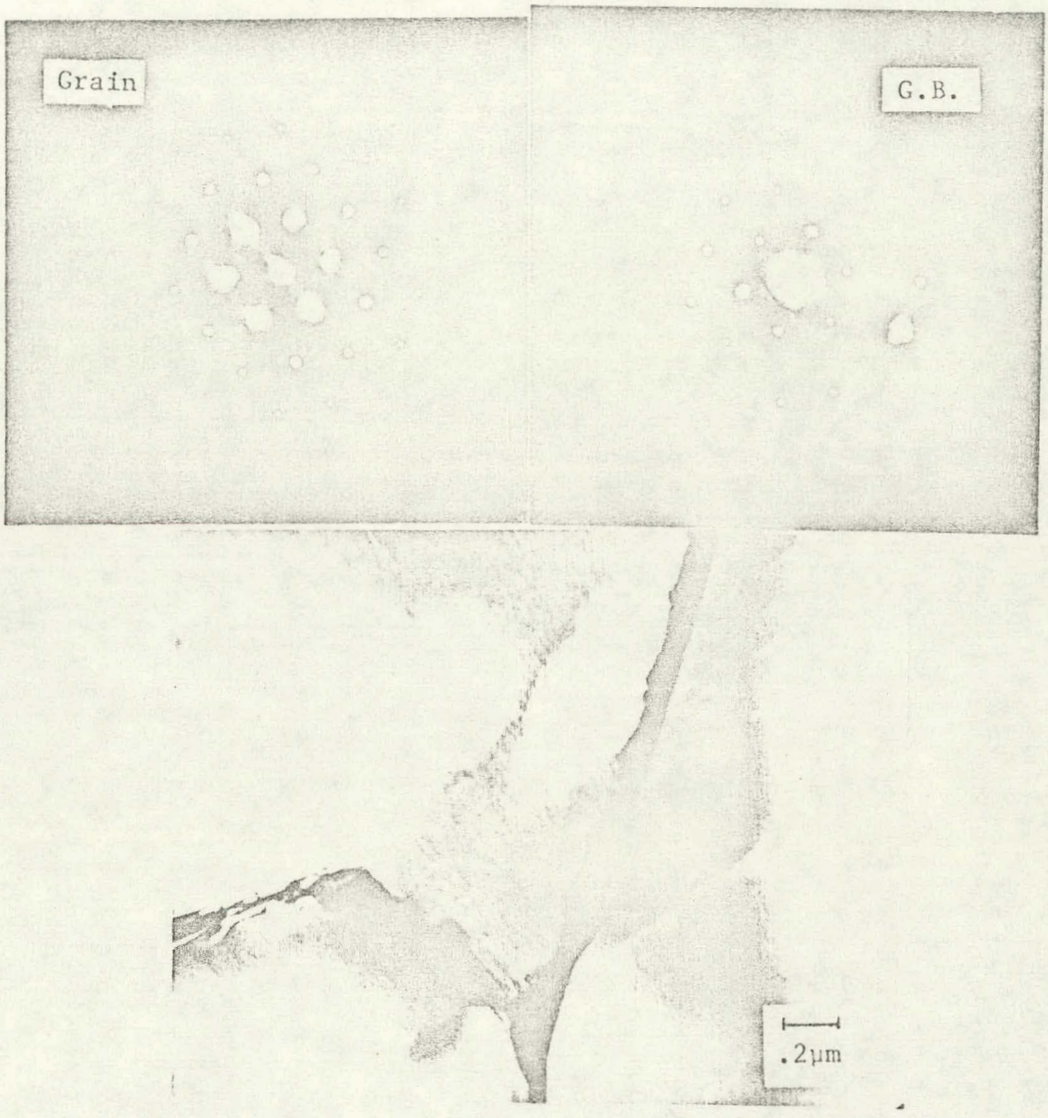

FIGURE 10. STEM photomicrograph and electron diffraction patterns for $SrTiO_3$ IBL capacitor prepared by ion-milling method.

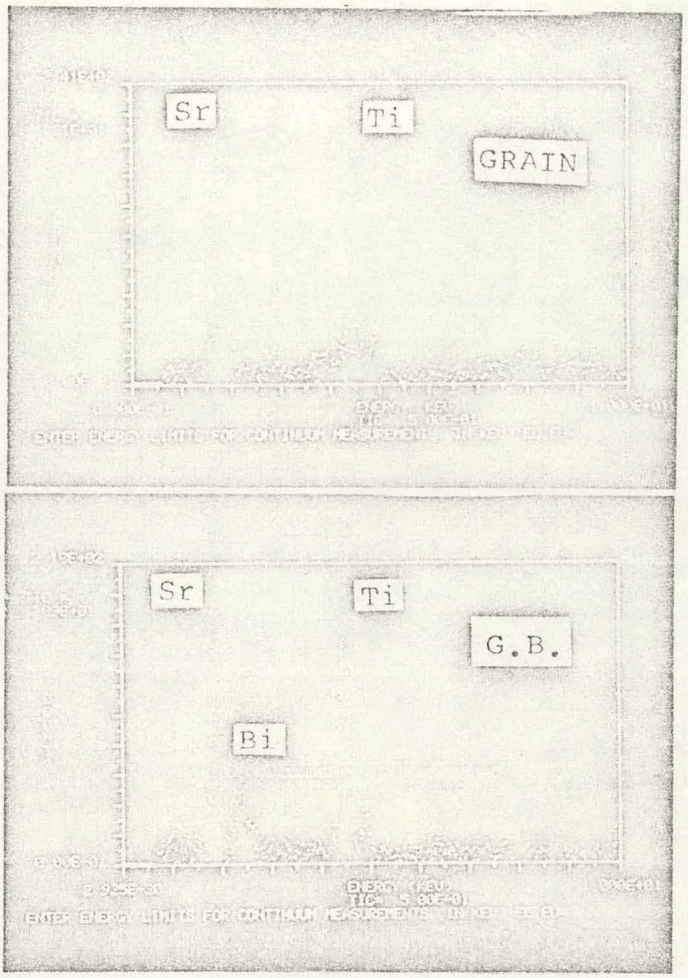

FIGURE 11. X-ray energy dispersive analysis of an IBL capacitor based upon $SrTiO_3$.

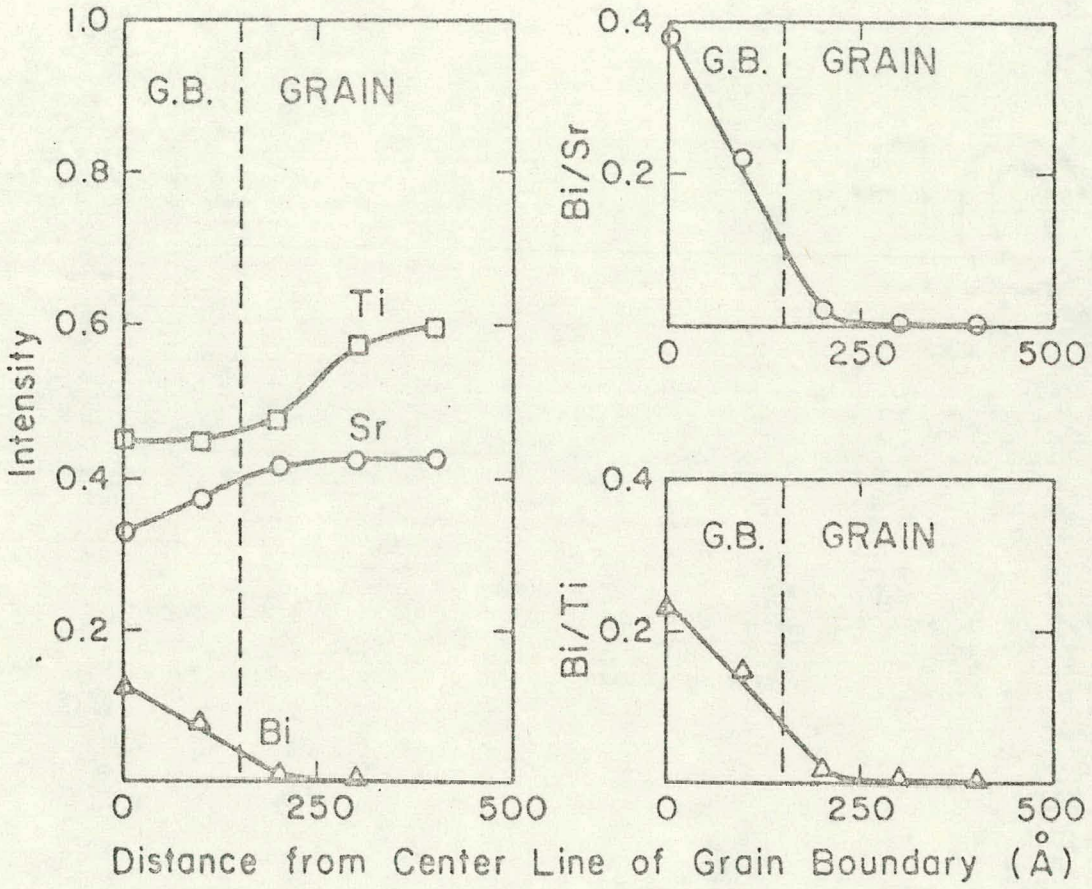

FIGURE 12. Concentration profiles of grain boundary region in a $SrTiO_3$ IBL capacitor.

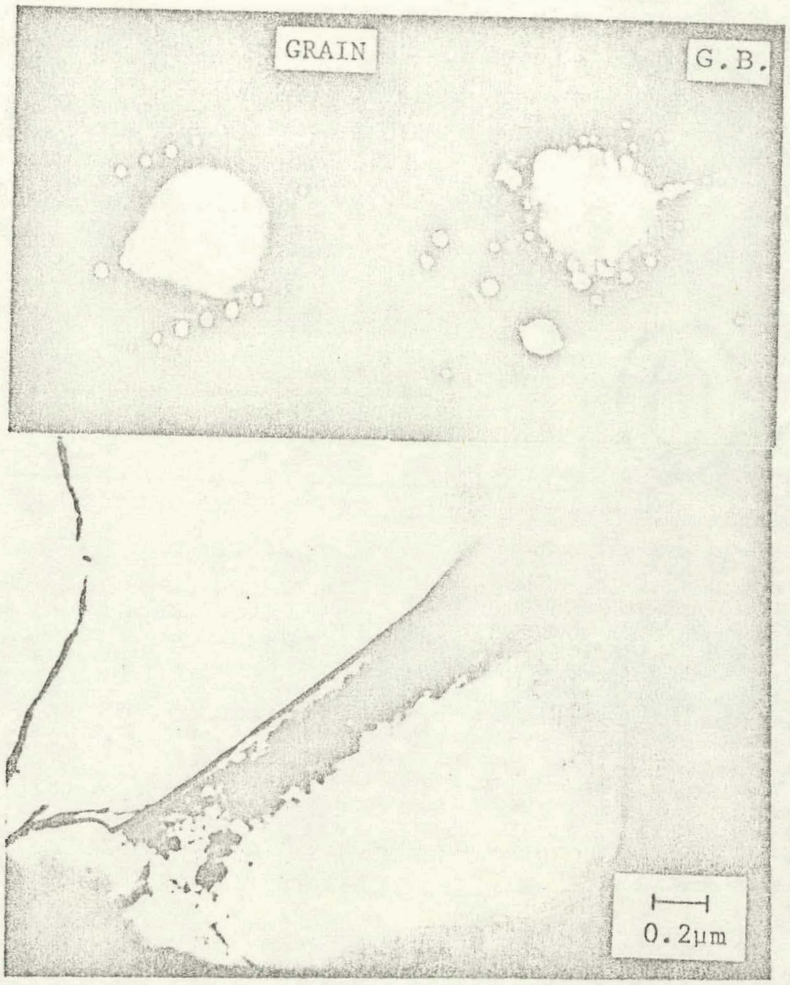

FIGURE 13. TEM photomicrograph and electron diffraction patterns of a $SrTiO_3$ IBL capacitor acceptor-doped with Cu.

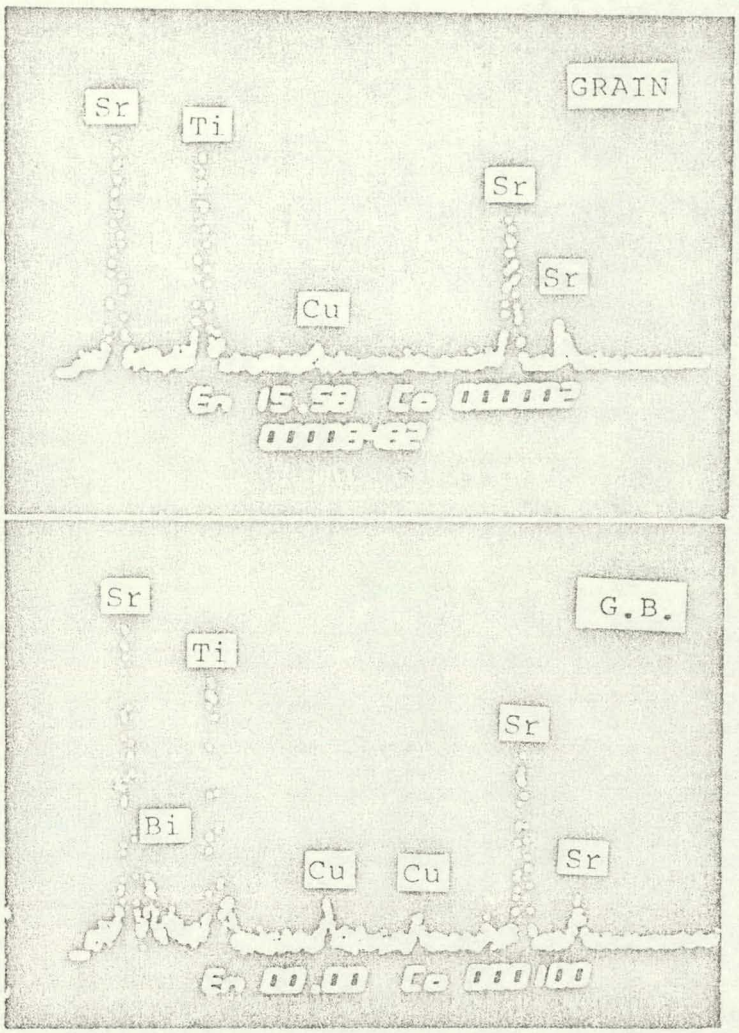

FIGURE 14. X-ray energy dispersive analysis of a $SrTiO_3$ capacitor acceptor-doped with Cu.

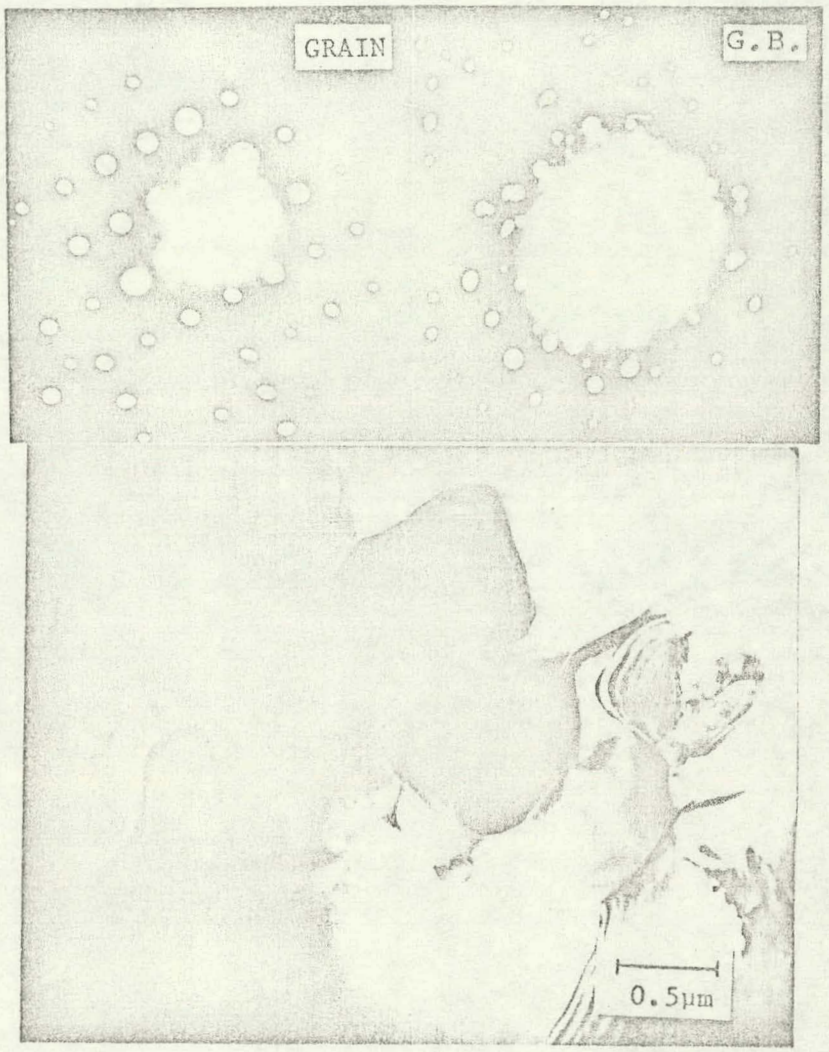

FIGURE 15. TEM photomicrograph and electron diffraction patterns of a $SrTiO_3$ IBL capacitor with a n-i-n structure.

diffraction. IBL capacitors (type I),formed by liquid phase sintering reduced $SrTiO_3$ powder with $Pb_5Ge_3O_{11}$, were found to have a much finer microstructure (Figure 15). The final grain size was essentially the same as the starting particle size, which ranged from 0.5-2 μm. This microstructure was suitable for thin layer multilayer capacitors. X-ray energy dispersive analysis (Figure 16) identified Pb to be within the boundary region.

B. Electrical Measurements

1. Current-voltage Characteristics

Current-voltage characteristics of the bulk specimen, of a single grain and boundary region are illustrated in Figures 17-19. The grains were ohmic in their I-V characteristics,whereas the boundaries were highly nonohmic,especially in the voltage range above 10V. The voltage dependent resistance (VDR) characteristics of the bulk,could be modeled on a series network of resistive distributed boundaries. I-V characteristics of IBL capacitors based upon $BaTiO_3$ were similar to those based on $SrTiO_3$, but the resistance of the grains were greater. Breakdown voltages for single junctions were about 65 volts for $SrTiO_3$ dielectrics, and about 400 volts for $BaTiO_3$ dielectrics. Considering the thickness of the intergranular layers (0.1 μm), the breakdown fields were 6.5×10^6 V/cm for $SrTiO_3$ based materials and 4×10^7 V/cm for $BaTiO_3$ based materials.

2. Current-temperature Characteristics

Typical data for the temperature dependence of resistivity for J-1 type IBL capacitor are given in Figure 20. Calculated resistivities indicate the boundary resistivities to be approximately

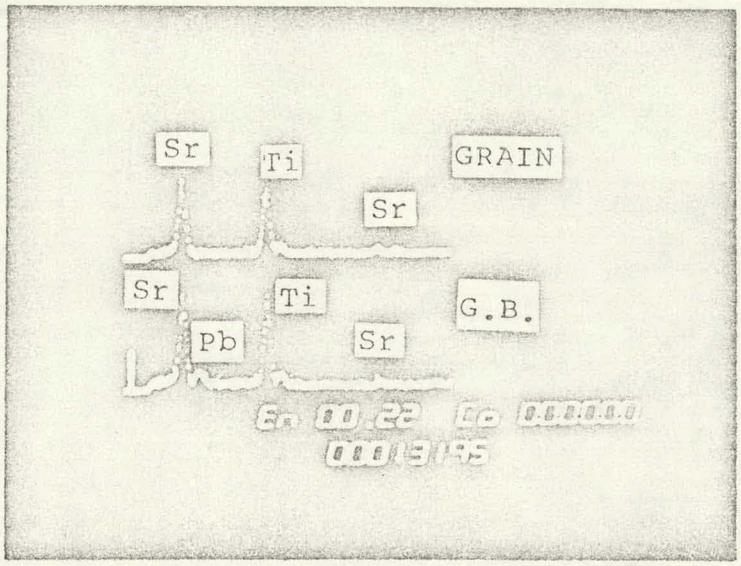

FIGURE 16. X-ray energy dispersive analysis of a $SrTiO_3$ IBL capacitor with a n-i-n structure.

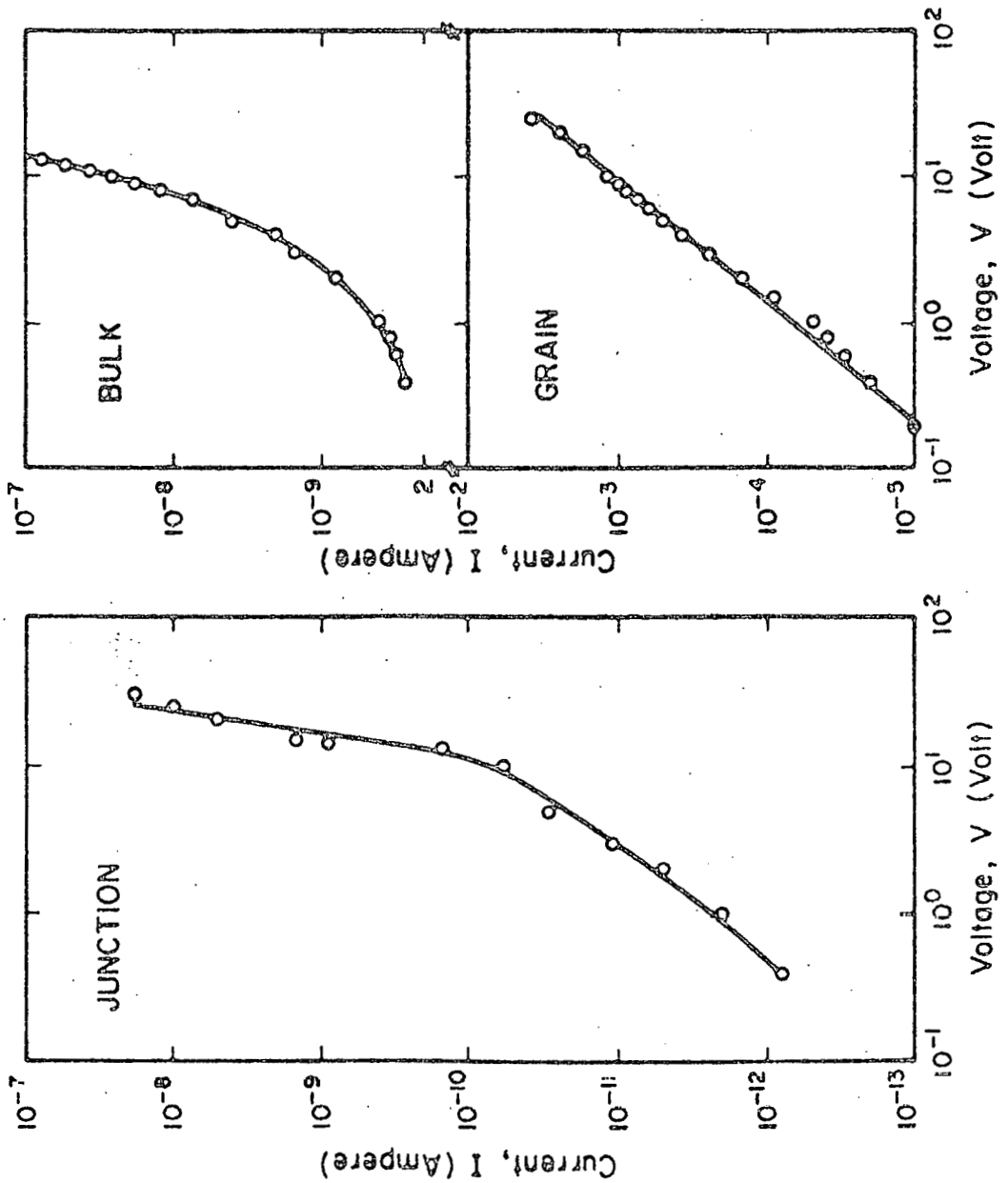

FIGURE 17. Current-voltage measurements: individual grain, boundary and bulk characteristics for a $SrTiO_3$ IBL capacitor (J-1).

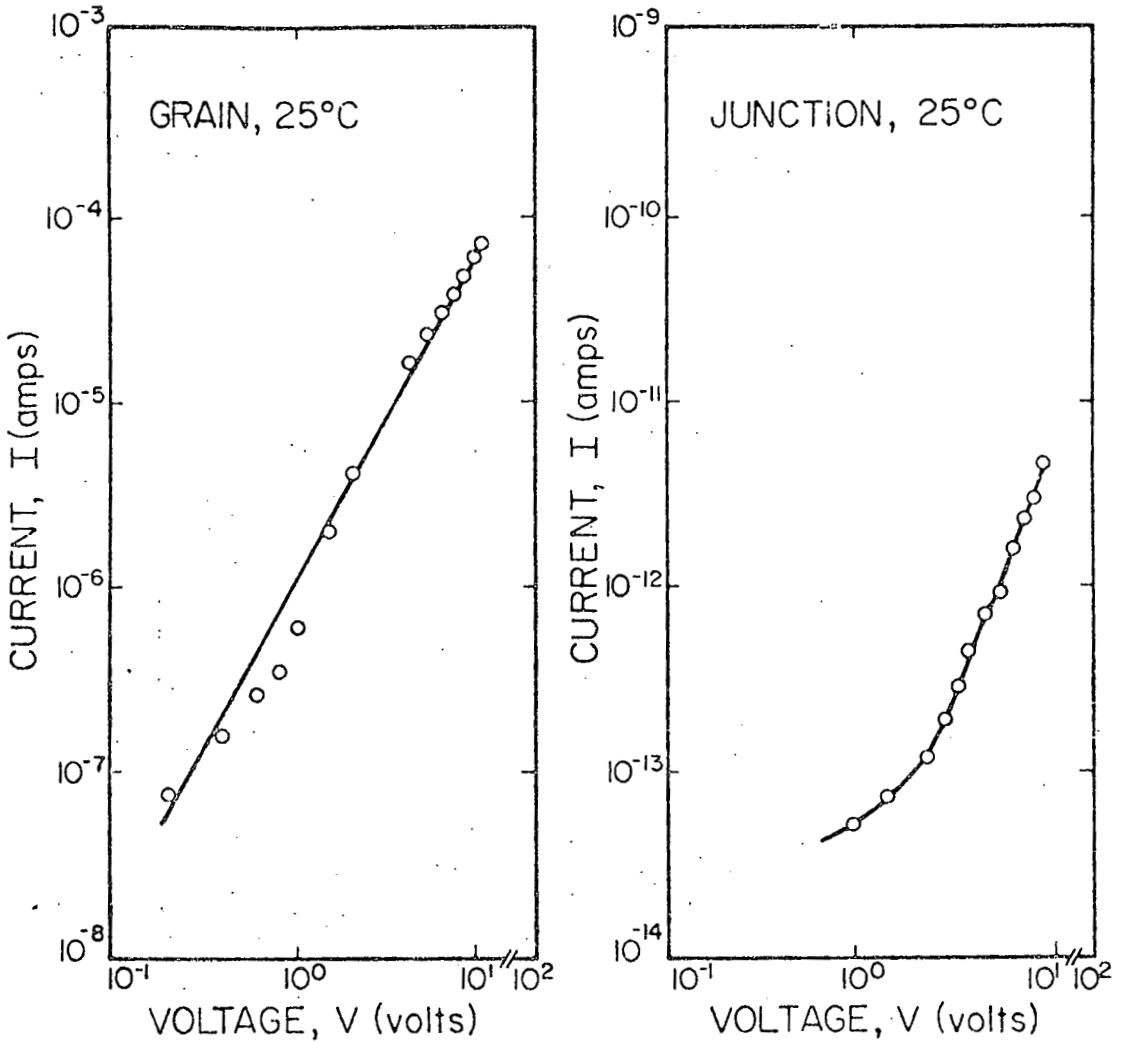

FIGURE 18. Current-voltage measurements of individual grain and boundary region in a $BaTiO_3$ IBL capacitor (G).

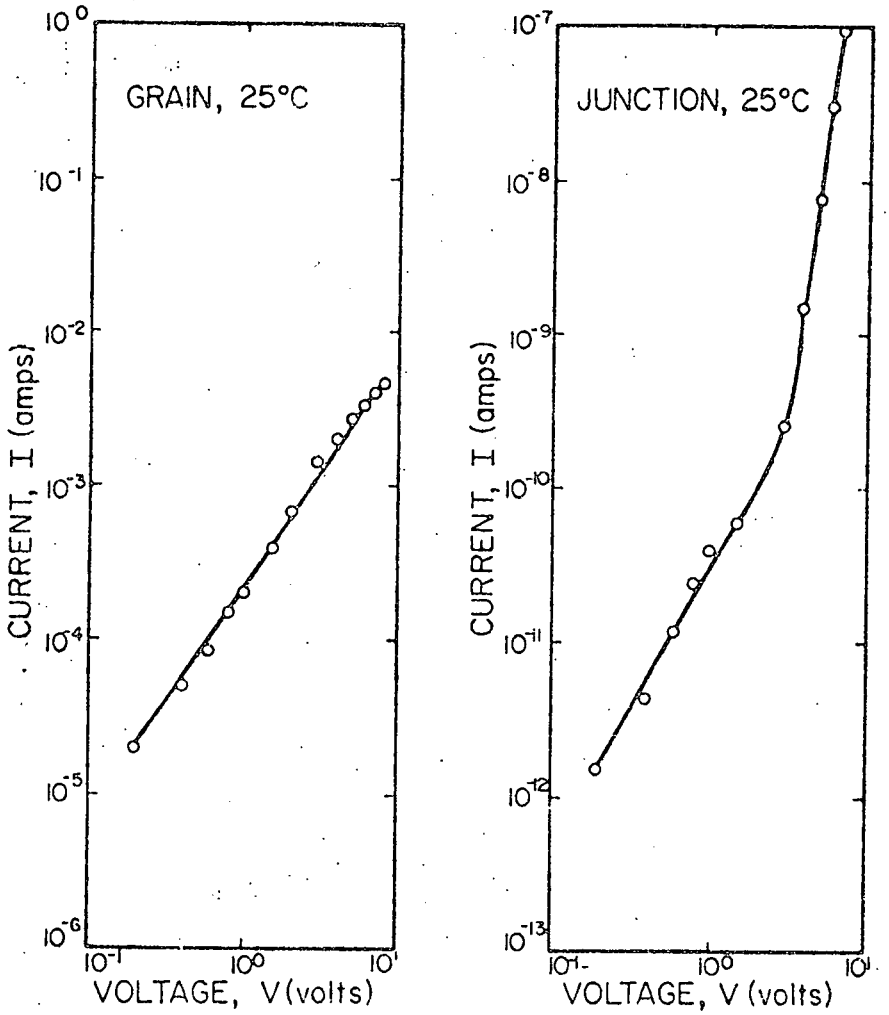

FIGURE 19. Current-voltage measurements of an individual grain and boundary region in a $SrTiO_3$ IBL capacitor (J-2).

10^{10} Ω-cm at room temperature, with a grain resistivity of approximately 50 Ω-cm. The insulating grain boundary resistivity was more temperature dependent than the semiconducting grain resistivity.

3. Capacitance-voltage Characteristics

Figure 21 illustrates the d.c. voltage dependence of dielectric constant for bulk samples. Dielectric saturation occurred readily, with increasing bias, for type G IBL capacitors. This is to be expected for ferroelectric materials based upon $BaTiO_3$. Temperature measurements (Figure 22) identified a dielectric transition close to room temperature, with a steep Curie-Weiss decay. Type G IBL capacitors were not stable in their properties as temperature and voltage varied, when compared with the behavior of $SrTiO_3$ based capacitors. The great advantage of microstructurally engineering IBL capacitors from paraelectric materials is self evident. In addition, $SrTiO_3$ type I IBL capacitors, which contained an insulating intergranular phase, and which approximated a n-i-n structure, were much more stable in their properties than commercial type J capacitors. The actual magnitude of $\bar{K}'$ depended on the volume fraction of liquid phase sintering compound used. Voltage dependent capacitance for individual boundaries are illustrated in Figure 23. Considering the actual boundary thickness from STEM micrographs of unetched specimens (0.01-0.1 μm), these measurements do not represent weak field values (i.e., 10^5 V/cm). The capacitance per boundary was approximately 10 pF, with a dissipation factor less than 4%. Capacitance voltage and capacitance-temperature measurements indicated the stability of n-i-n type I capacitors, and the voltage

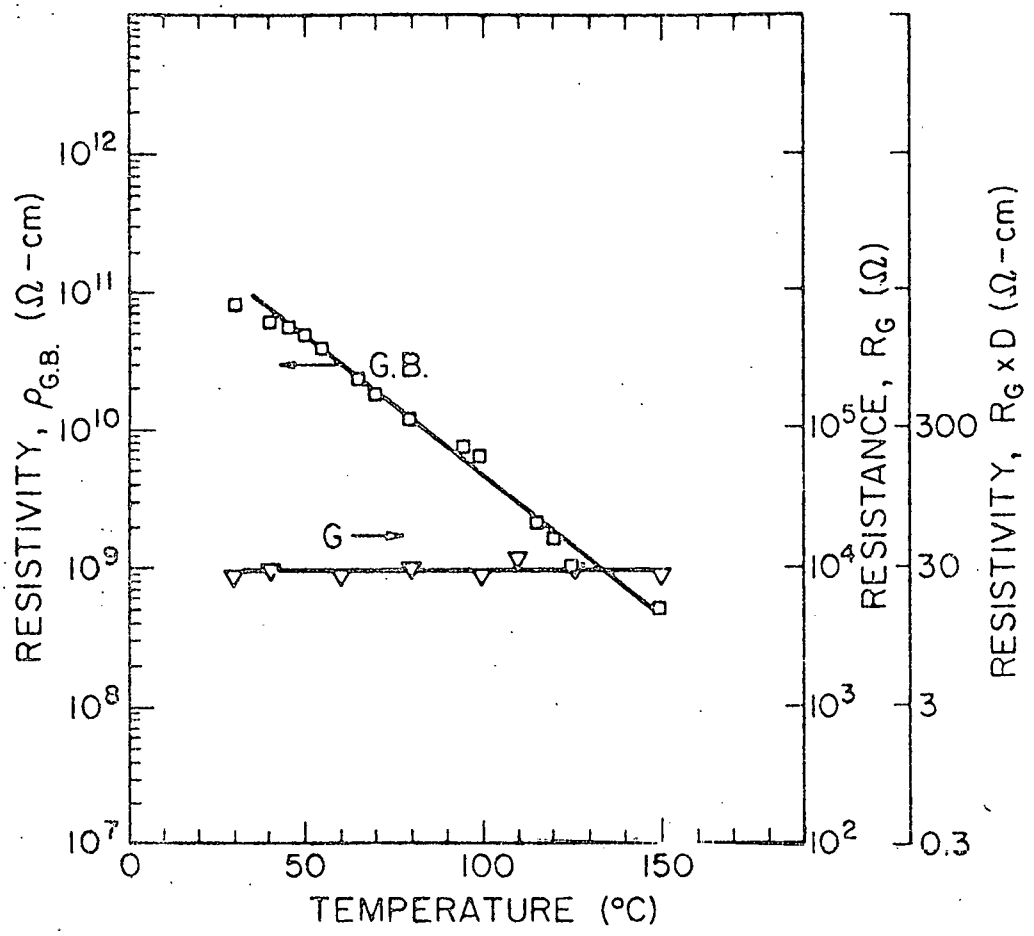

FIGURE 20. Resistivity as a function of temperature for a single grain and junction in an IBL capacitor.

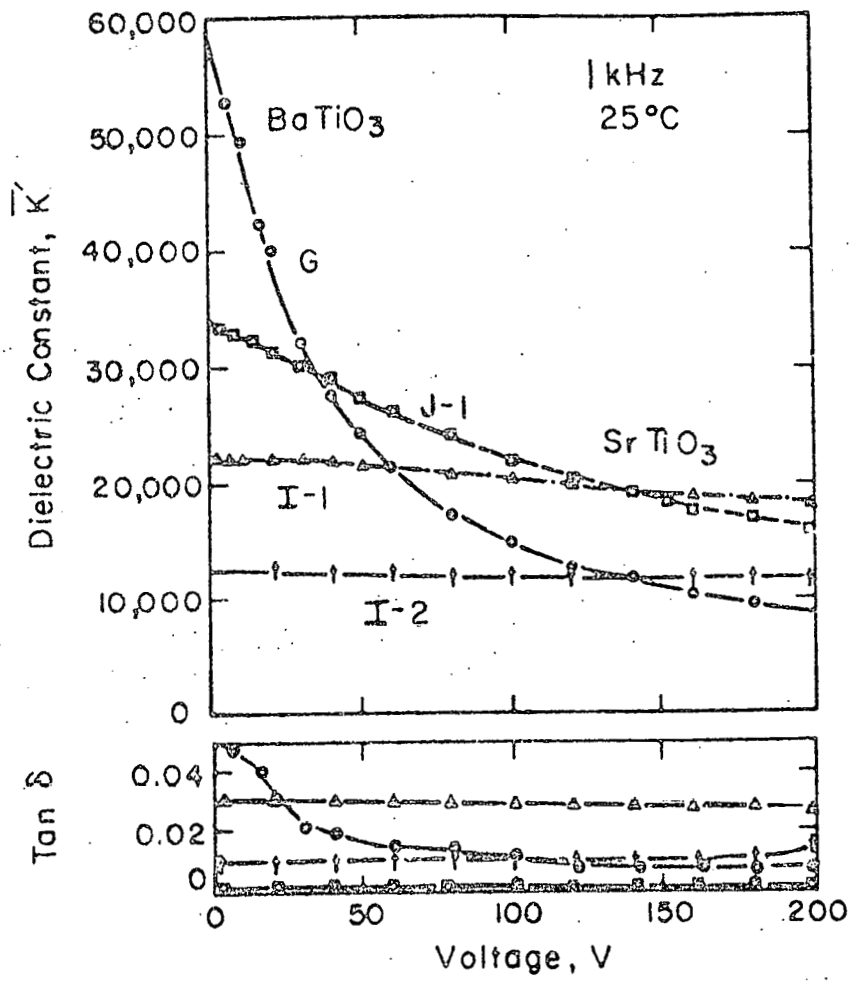

Figure 21. D.C. bias-voltage dependence of dielectric properties for several internal boundary layer capacitors

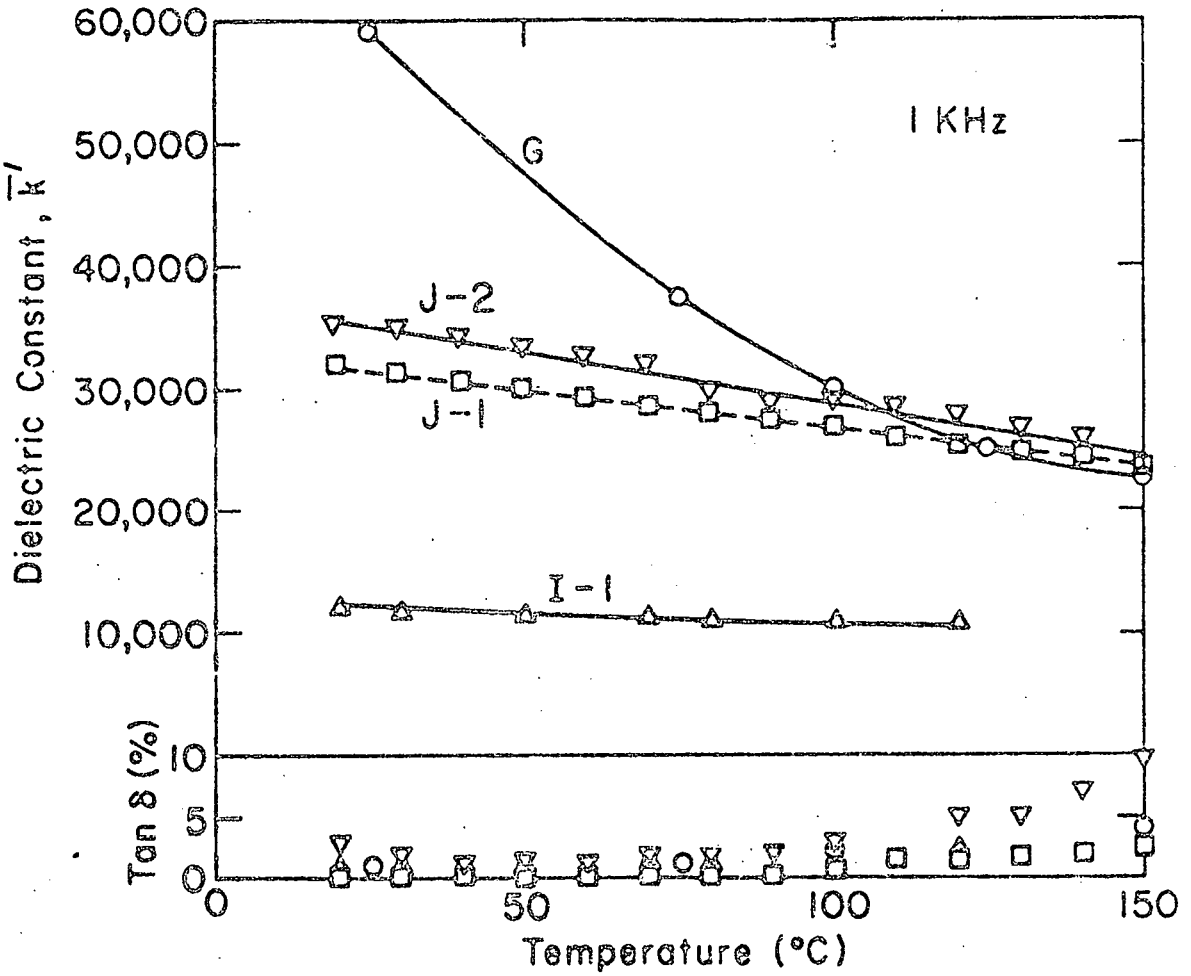

FIGURE 22. Temperature dependent dielectric properties for IBL capacitors.

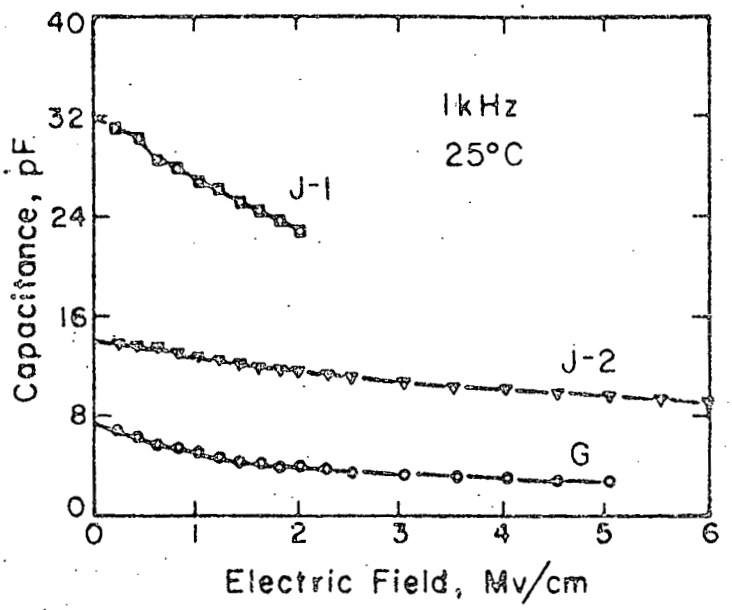

FIGURE 23. Capacitance of a single junction as a function of electric field for IBL capacitors.

dependence of commercial dielectrics (G and J). Measurements on the latter were made both of the bulk and boundary characteristics, and the data analyzed in terms of step (C^{-2} vs. V) or graded (C^{-3} vs. V) junctions. Unambiguous analysis appeared at first to be not possible. Data given in Figure 24 are for various types of IBL capacitors. It may be interpreted that high voltage characteristics are approximated by Schottky type depletion layer behavior, and the low voltage characteristics by insulation stabilization. A hybrid model, developed to account for these overall characteristics, will be presented in the following chapter.

4. Dielectric Dispersion

Figures 25-27 illustrate the single junction capacitance vs. frequency characteristics of IBL capacitors. Capacitance decreases over a wide range of frequency, and a broad peak for tan δ indicates the possibility of more than one relaxation process. Tan δ peaks at approximately 10^6 Hz for capacitor G, and in the gigahertz range for capacitors based upon $SrTiO_3$ (J-1, J-2).

Cole-Cole plots for single junctions are shown in Figures 28-30. The plots may be interpreted in terms of two relaxation processes. The conductivity increases in the lower frequency range, and the dielectric loss (in which the d.c. conductivity contribution was subtracted out) is also given in Figures 28-30. Dielectric dispersion behavior and corresponding Cole-Cole plots for polycrystalline bulk capacitors are illustrated in Figures 31-38. K' vs. frequency plots for J-1 and J-2 IBL capacitors indicate a relaxation may occur in the gigahertz range, but it was difficult to analyse the Cole-Cole plots due to a lack of experimental high frequency data (> 100 MHz).

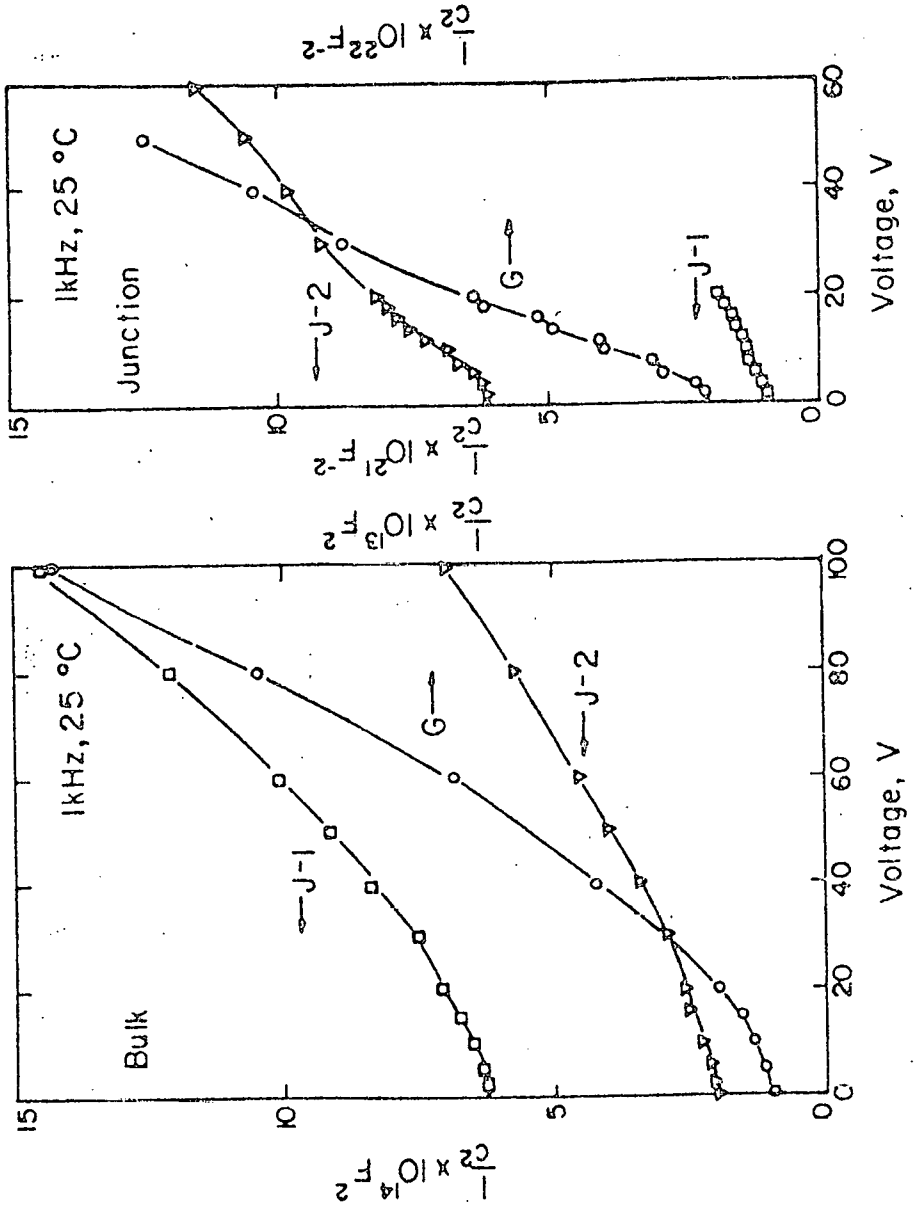

FIGURE 24. Voltage dependent capacitance of IBL capacitors.

Dielectric dispersion behavior of polycrystalline IBL capacitors based on G exhibited a typical single Debye-type relaxation, with a relaxation frequency around 10^6 Hz. Two layer n-i-n capacitors (I-1 and I-2) showed typical Maxwell-Wagner dispersion behaviors, in which the relaxation frequencies were around 30-50 MHz.

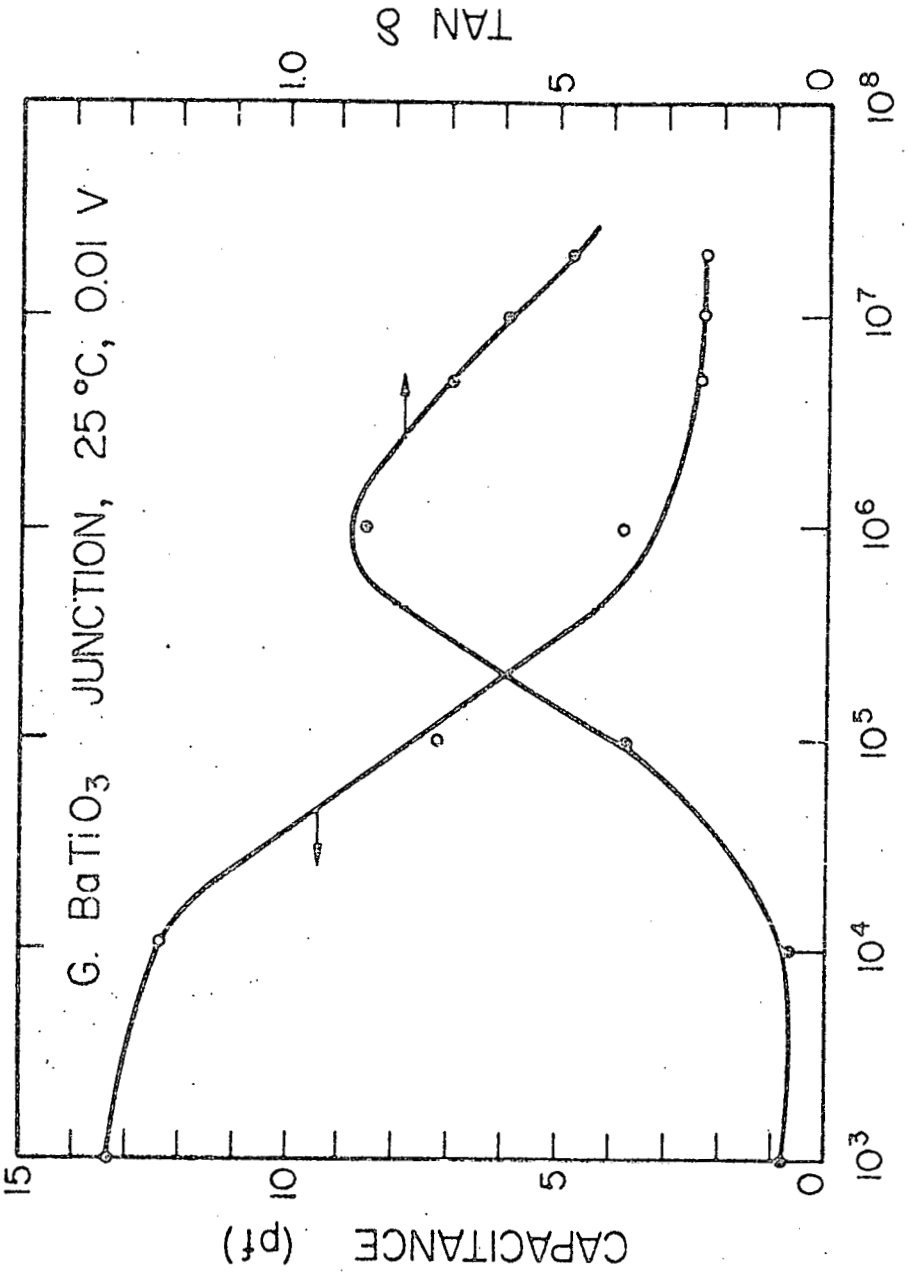

FIGURE 25. Fre uency de endent dielectric const

FIGURE 25. Frequency dependent dielectric constant and tan δ for a single junction in a $BaTiO_3$ IBL capacitor.

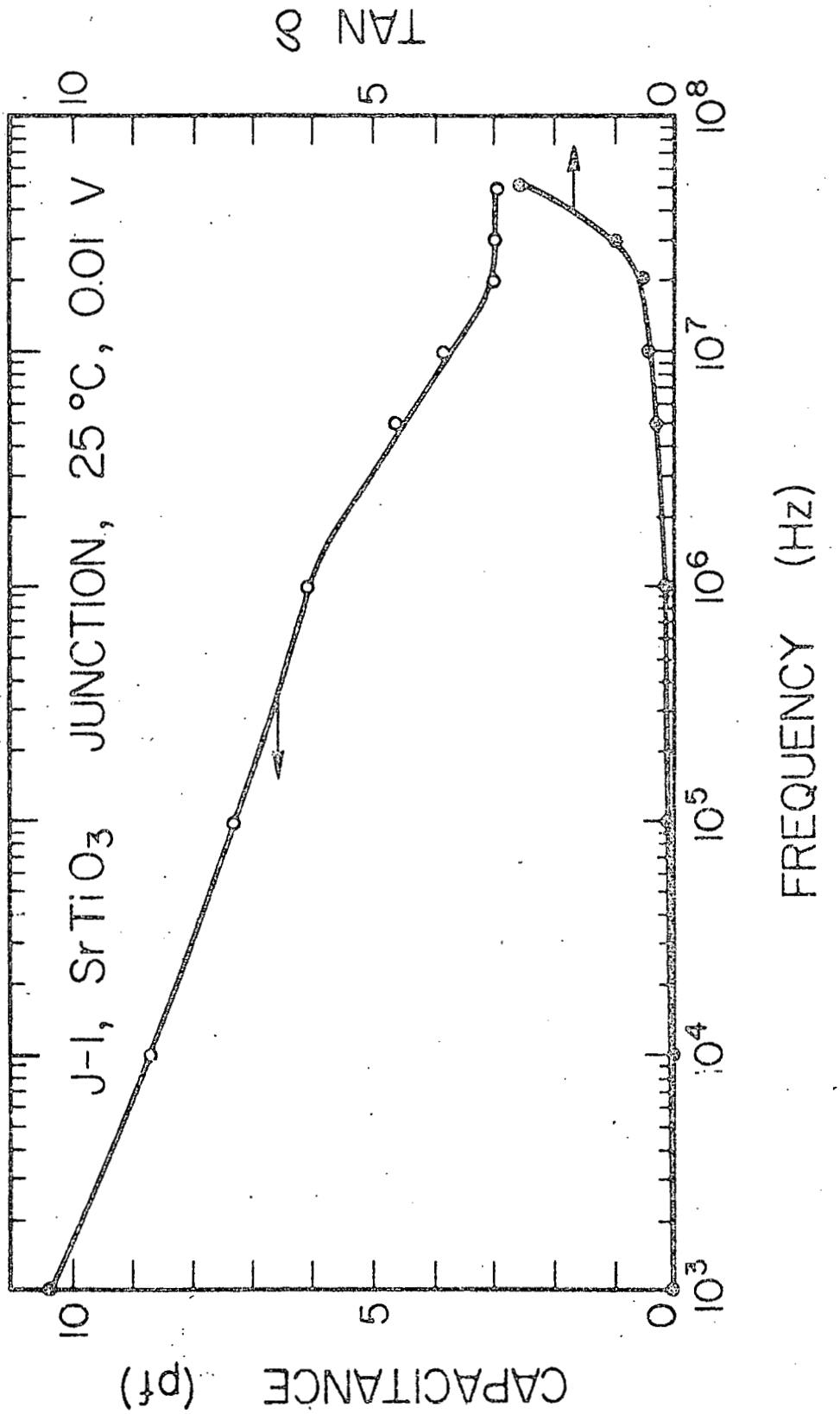

FIGURE 26. Frequency dependent dielectric constant and tan δ for a single junction in a $SrTiO_3$ IBL capacitor.

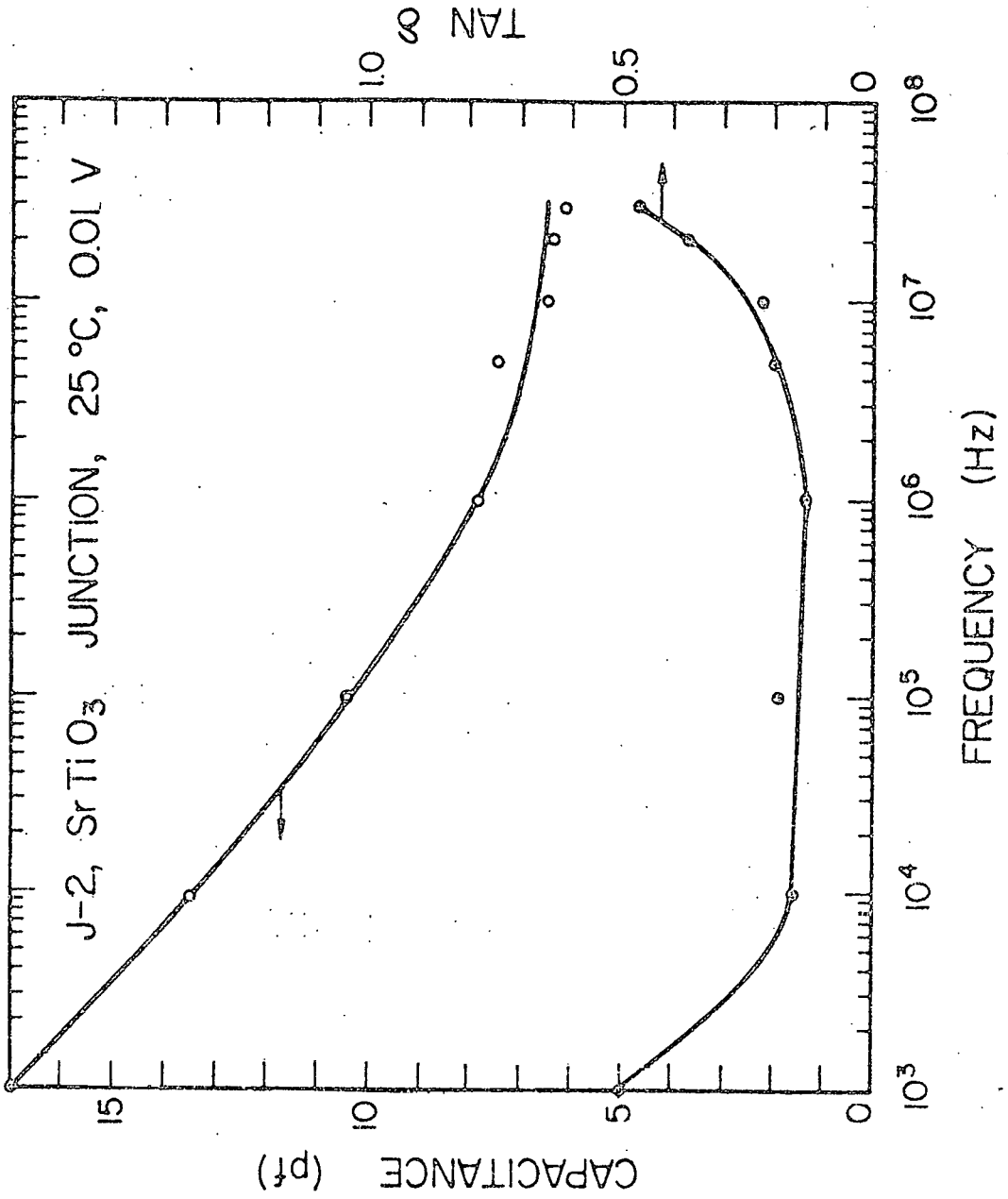

FIGURE 27. Frequency dependent dielectric constant and tan δ for a single junction in a $SrTiO_3$ IBL capacitor.

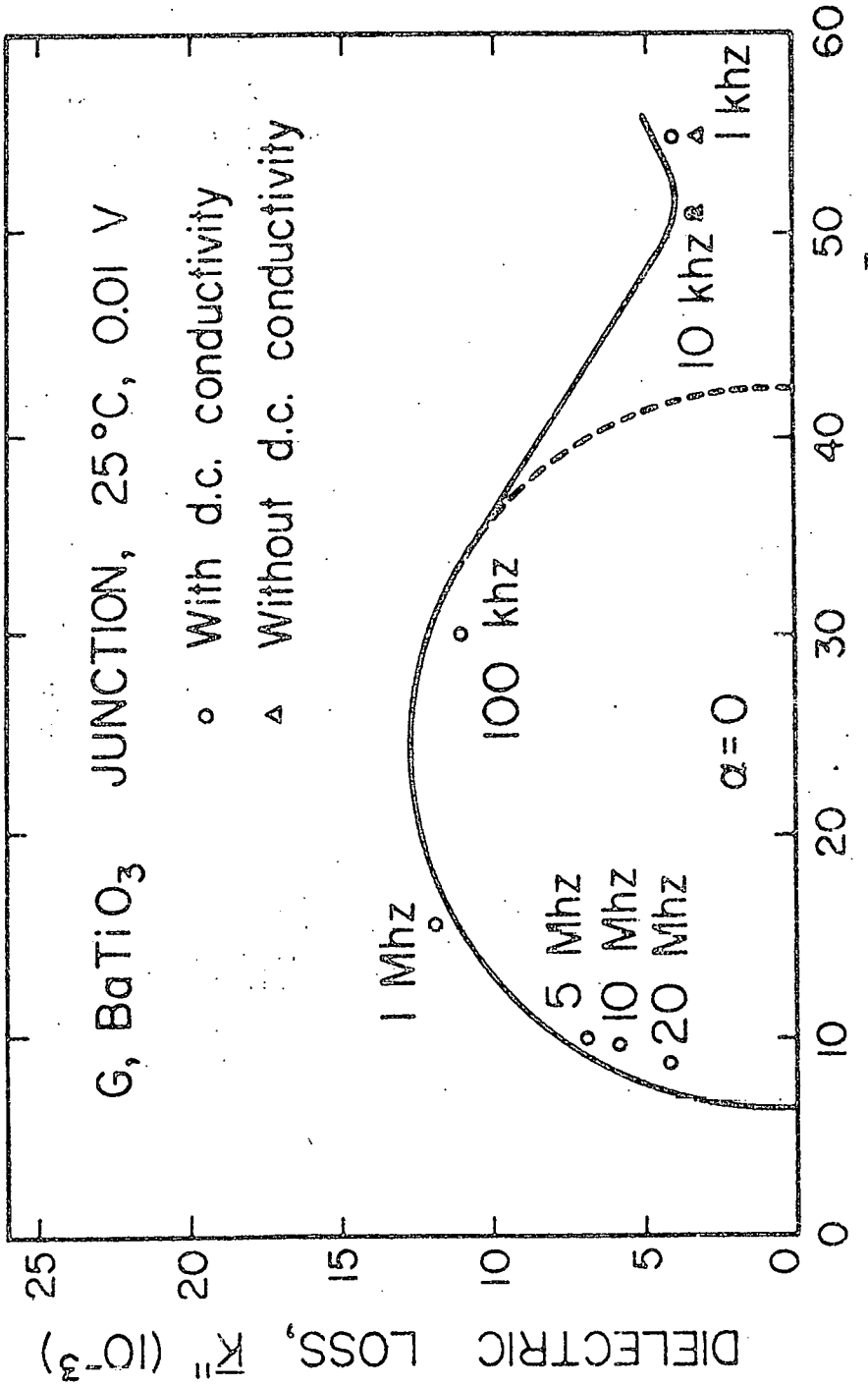

FIGURE 28. Cole-Cole plot for a single junction in a $BaTiO_3$ IBL capacitor.

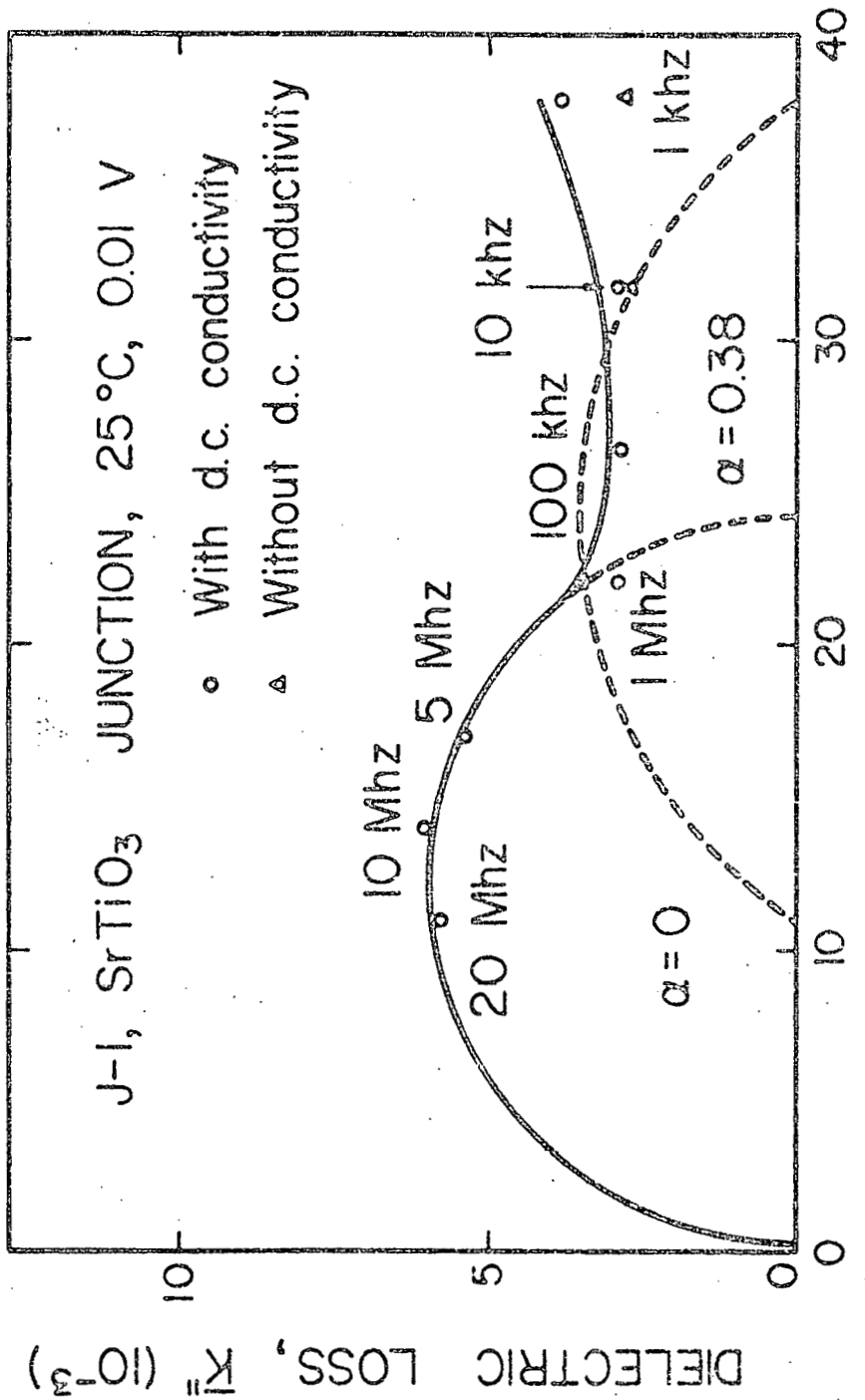

FIGURE 29. Cole-Cole plot for a single junction in a $SrTiO_3$ IBL capacitor.

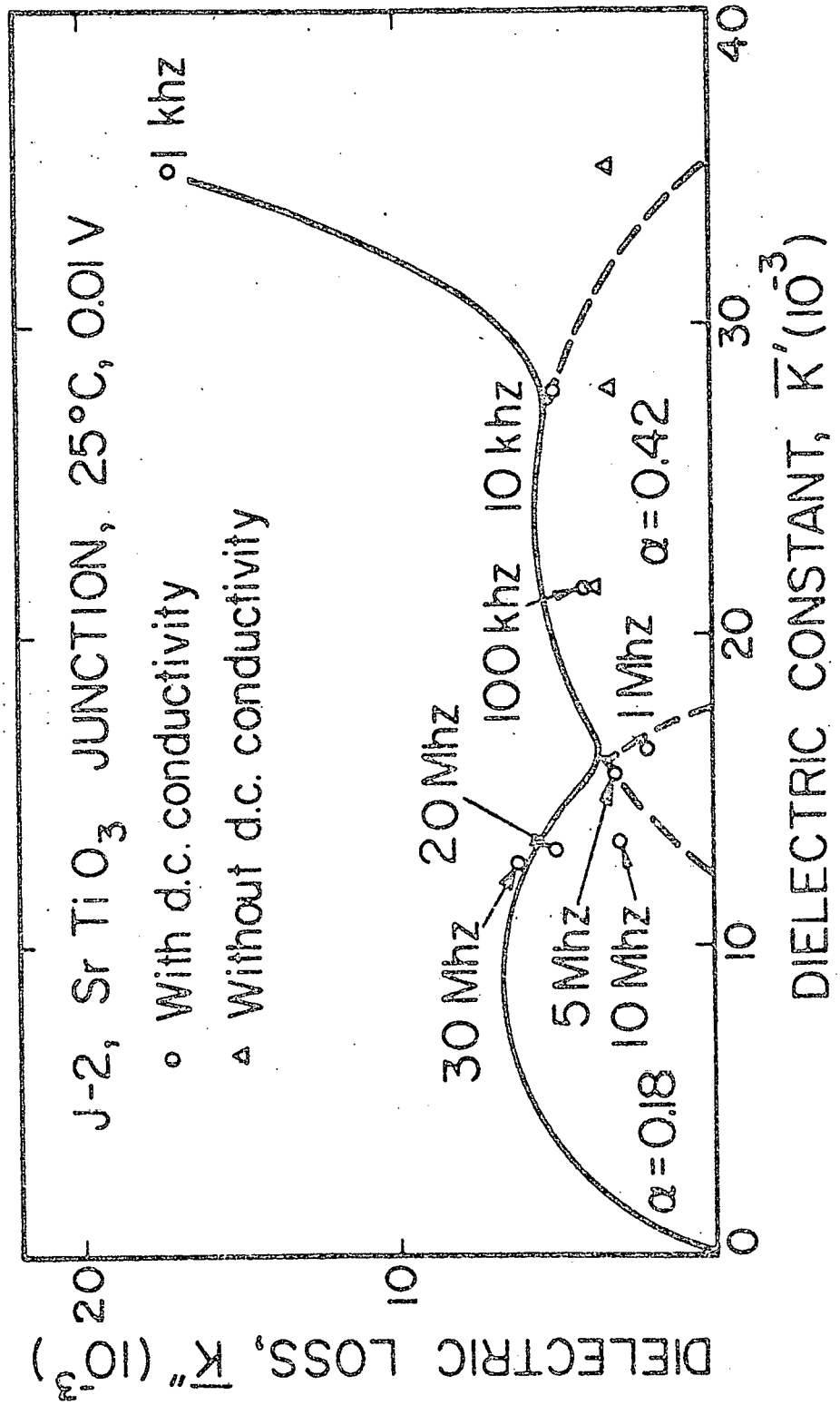

FIGURE 30. Cole-Cole plot for a single junction in a $SrTiO_3$ IBL capacitor.

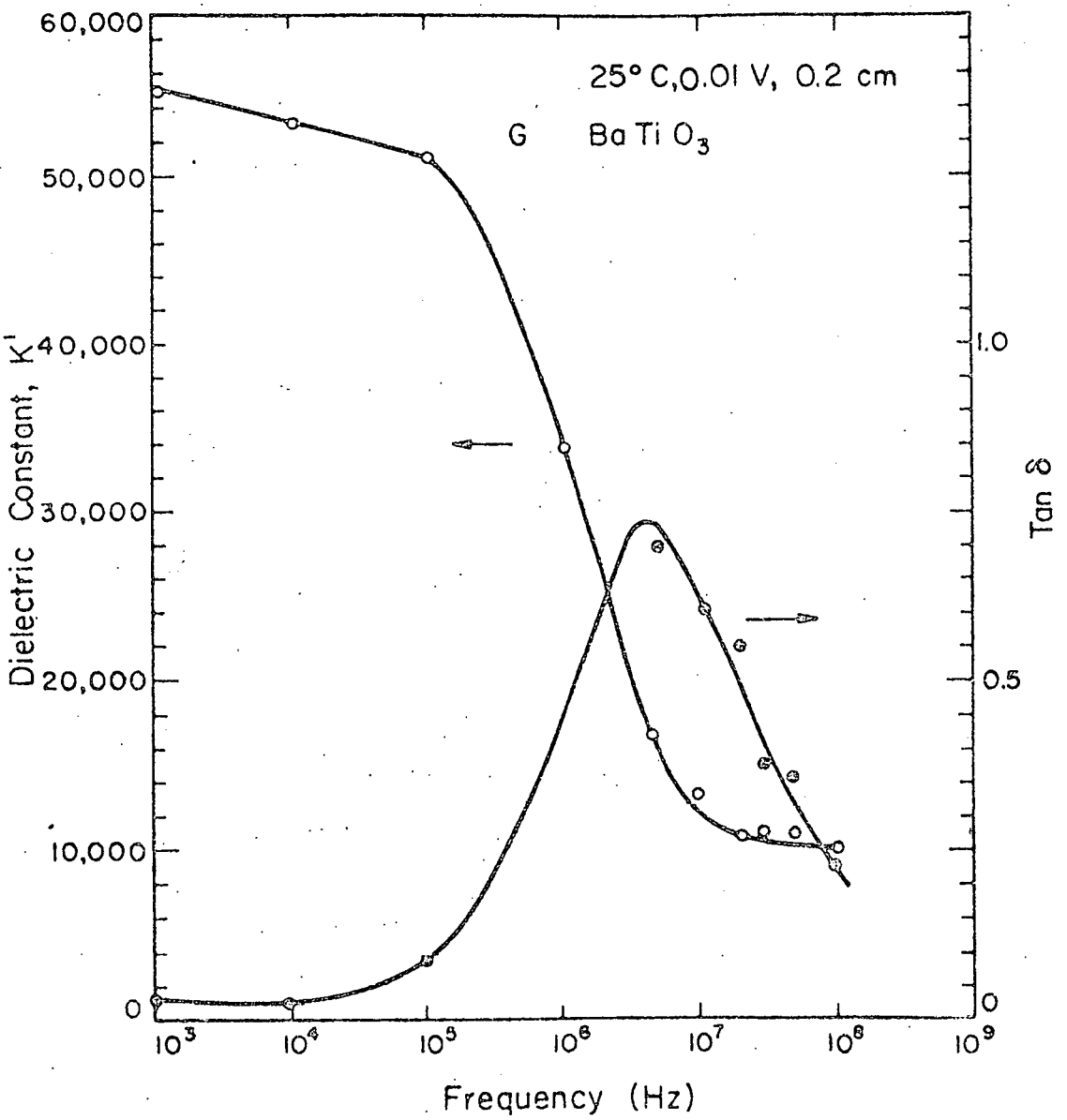

FIGURE 31. Frequency dependent dielectric constant and tan δ for a $BaTiO_3$ IBL dielectric

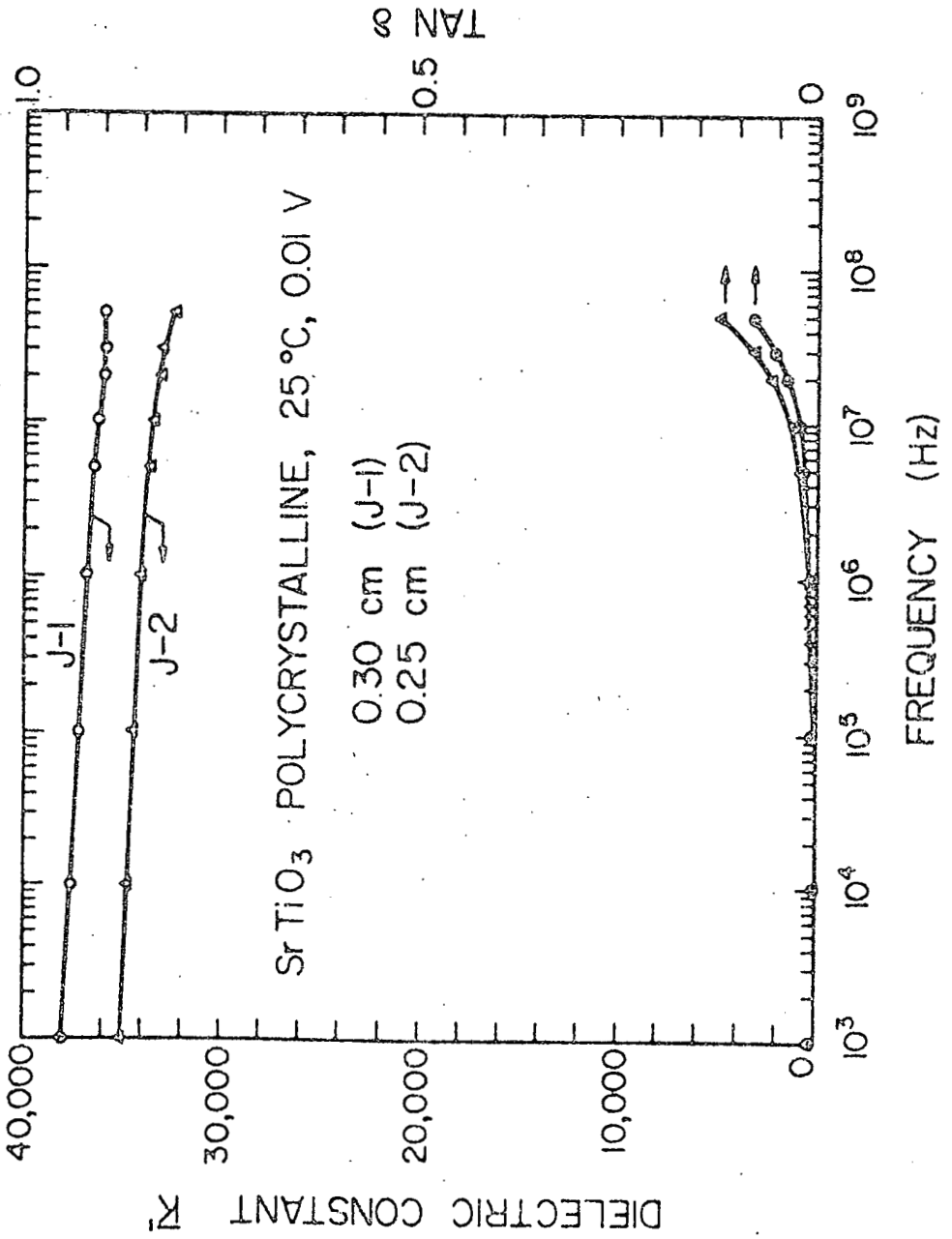

FIGURE 32. Frequency dependent dielectric constant and tan δ for a $SrTiO_3$ IBL capacitors.

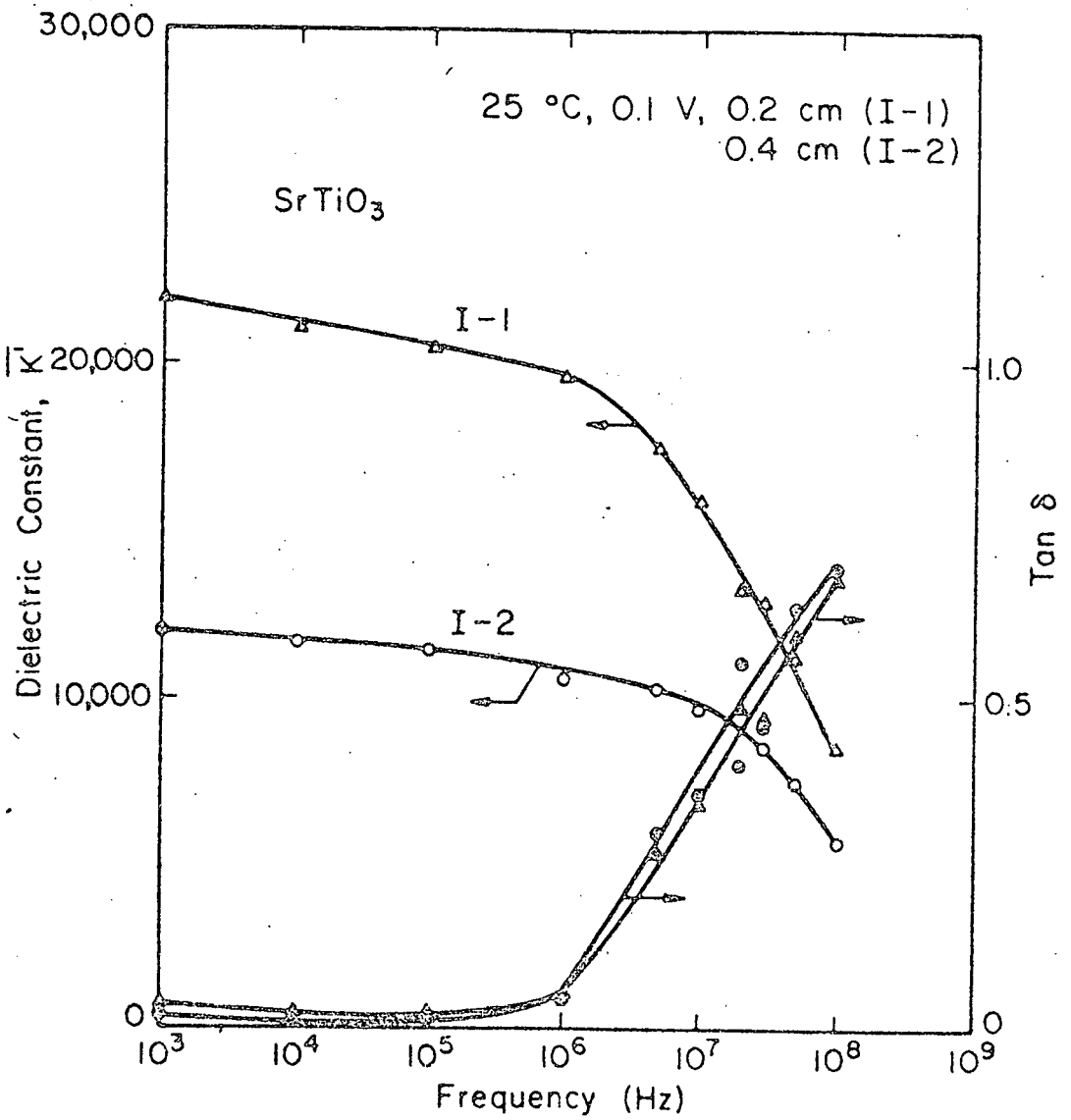

FIGURE 33. Frequency dependent dielectric constant and tan δ for a $SrTiO_3$ IBL capacitors.

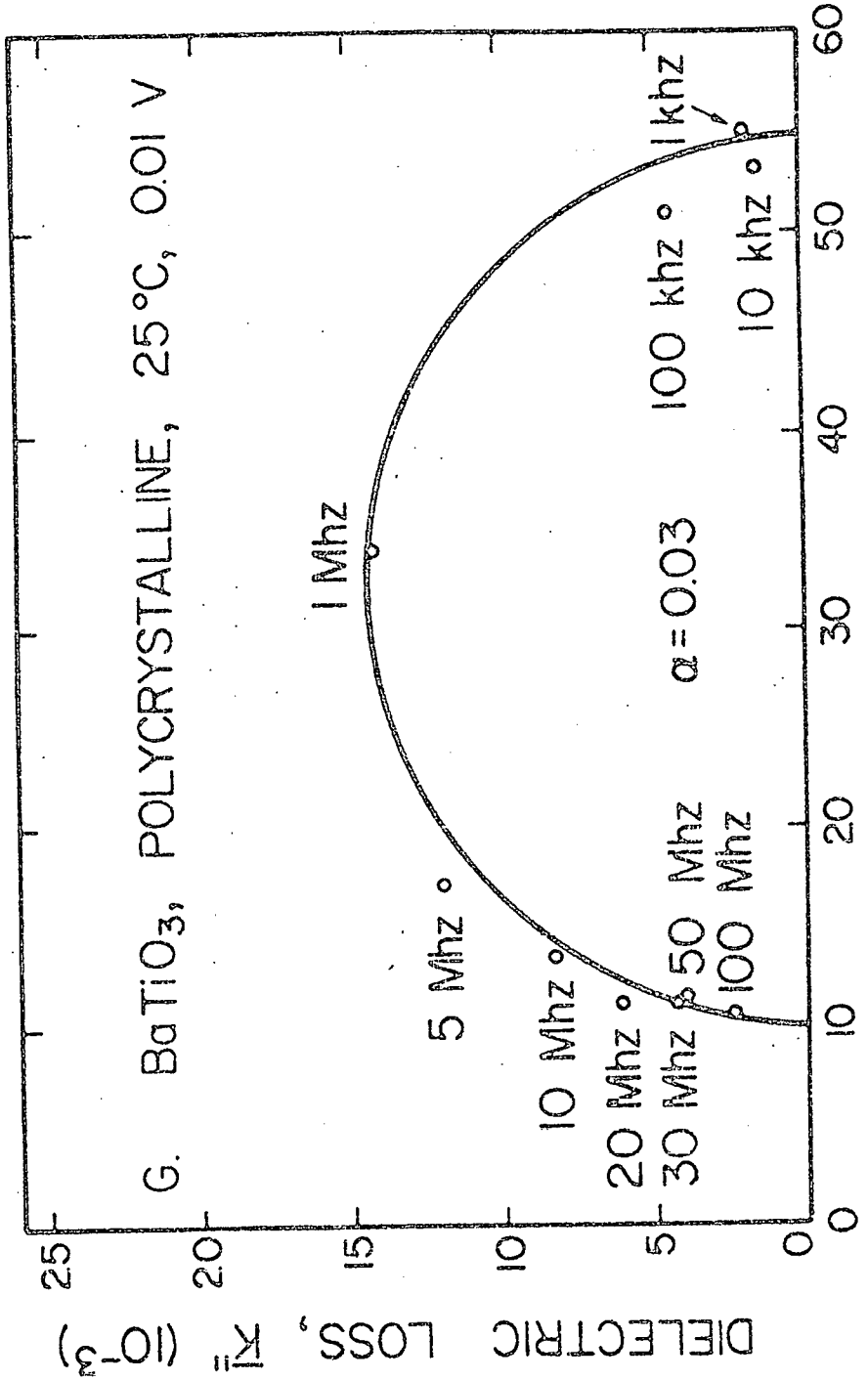

FIGURE 34. Cole-Cole plot for a $BaTiO_3$ IBL capacitor.

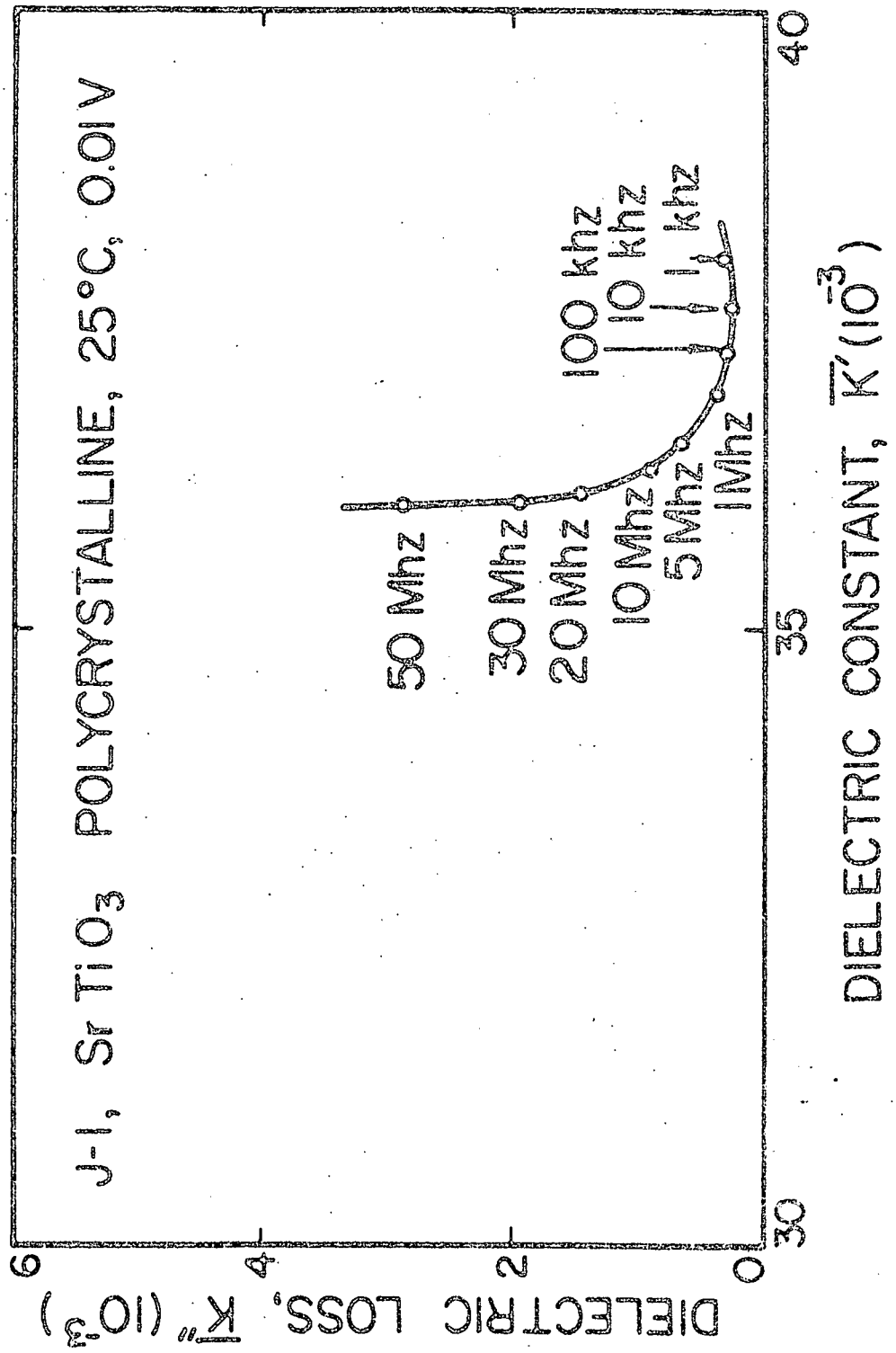

FIGURE 35. Cole-Cole plot for a $SrTiO_3$ IBL capacitor.

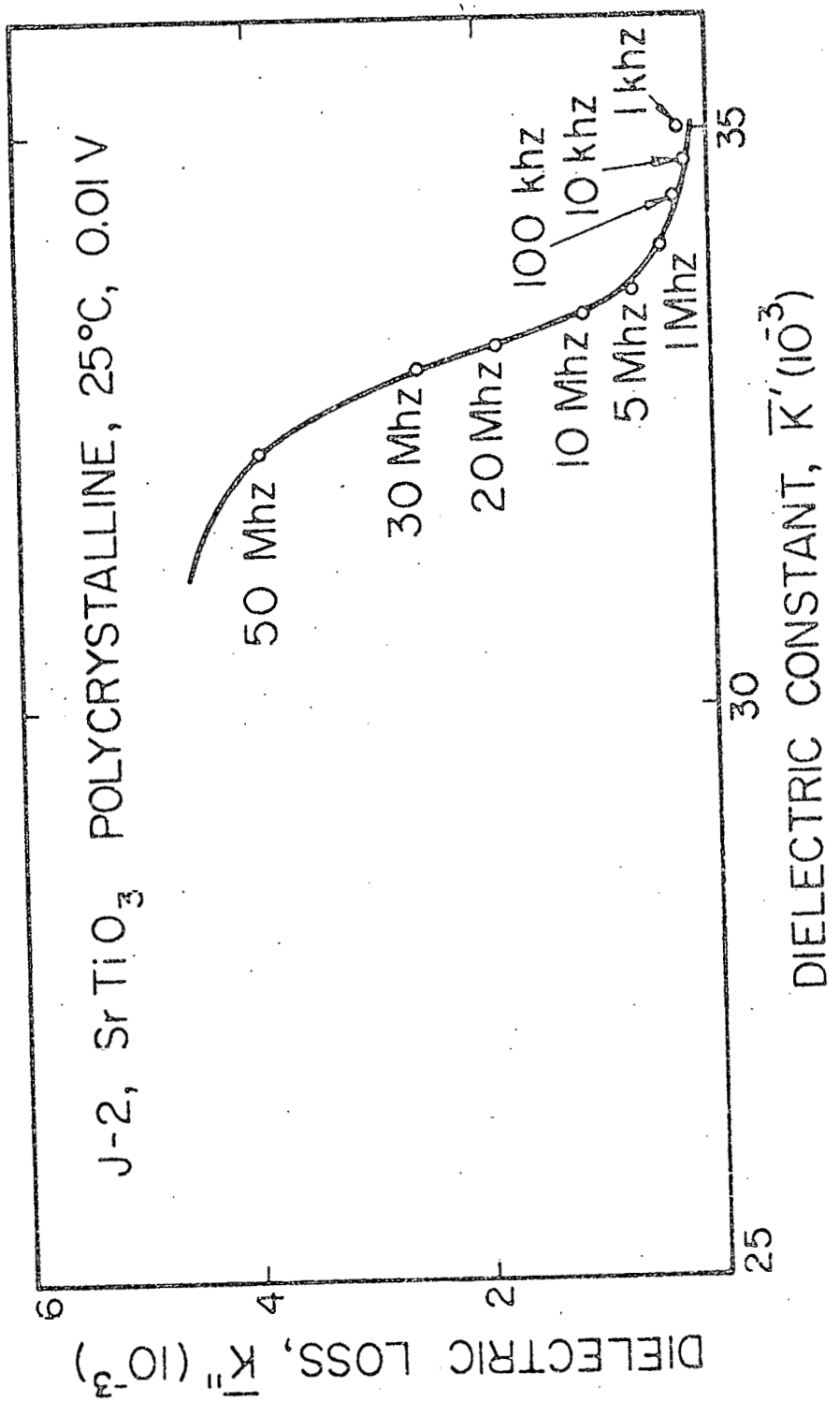

FIGURE 36. Cole-Cole plot for a $SrTiO_3$ IBL capacitor.

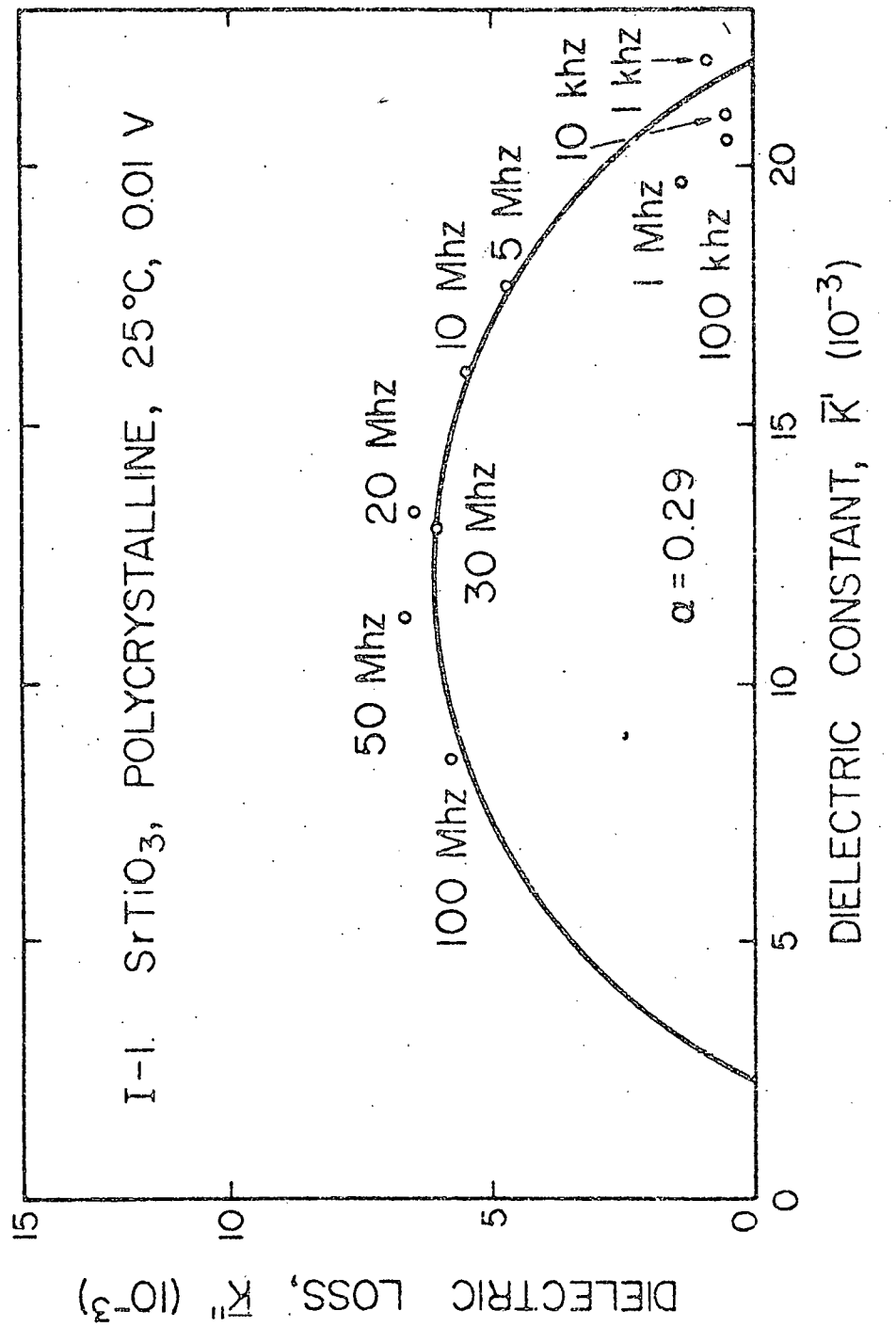

FIGURE 37. Cole-Cole plot for a $SrTiO_3$ IBL capacitor.

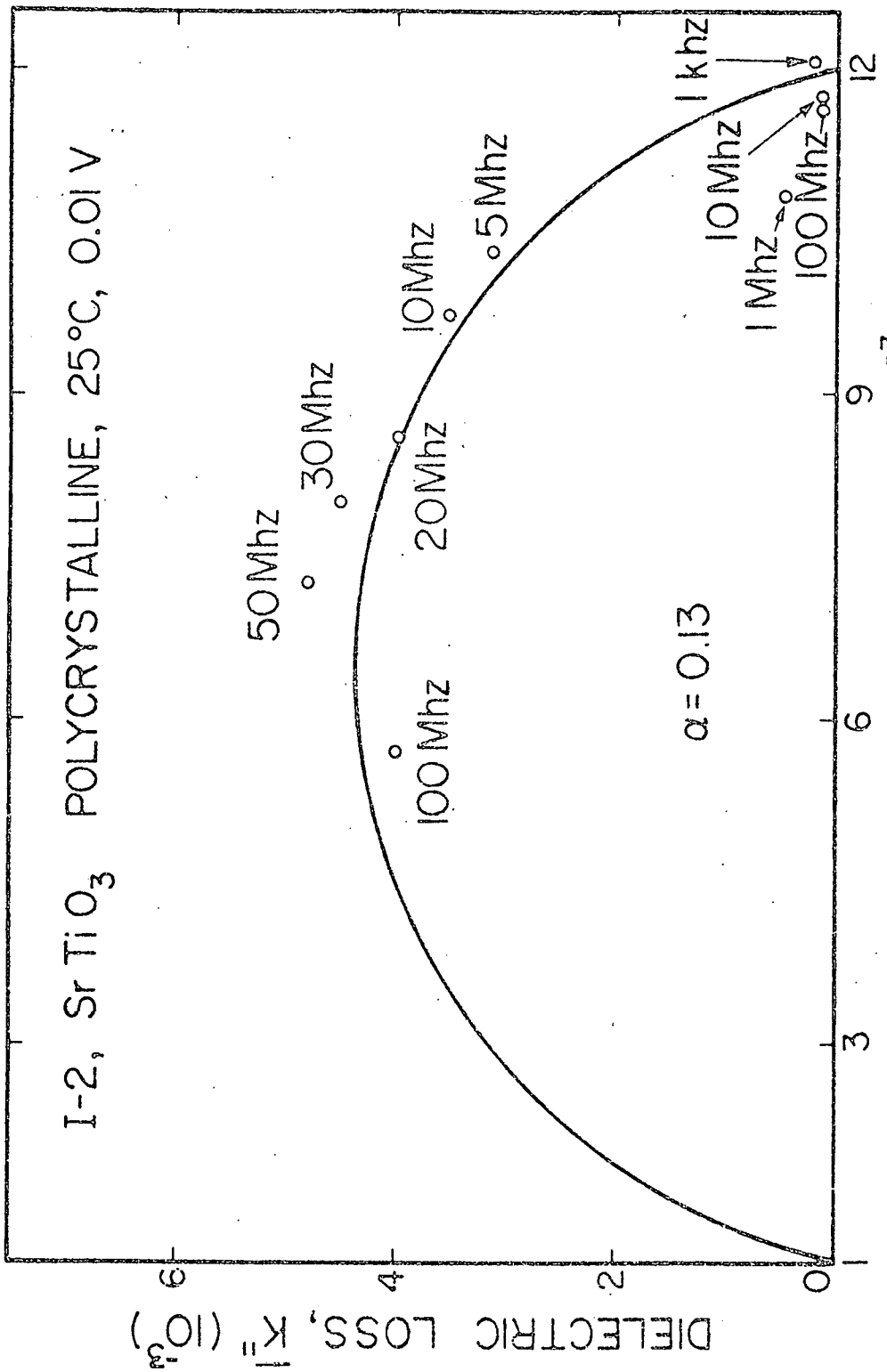

FIGURE 38. Cole-Cole plot for a $SrTiO_3$ IBL capacitor.

VI. DISCUSSION

A. Microstructure Analysis

The results of electron probe microanalysis for $BaTiO_3$ IBL capacitors, indicated a high titania rich boundary phase. Interpretation of the microstructure, with respect to the composition, phase diagram (given in Appendix A) and known sintering temperature (1380°C) indicated that $(Ba,Sr)(Ti,Sn)O_3$ grains were liquid phase sintered in the presence of a high titanate second phase, which crystallized on cooling. Dielectric analysis (see section VI-B) strongly supports the presence of an insulating $BaO \cdot nTiO_2$ second phase. The Al and Si content in the grain boundary regions indicated the possibility of small additions of clay minerals for plasticity in forming and enhanced vitrification in firing. Both Sn and Sr were added to shift the Curie point towards room temperature for enhancement of dielectric constant.

For type J $SrTiO_3$ IBL capacitors, microstructural observation demonstrated high Bi concentration in the grain boundary regions; and probe analysis determined the concentration profiles between resistive boundaries and semiconducting grains. The fabrication process for type-J IBL capacitors (i.e., a two step firing process), allowed a limited amount of the additives to diffuse into the grains (i.e., during the second firing), even though most of the additives remained between the grains, forming an insulating layer. At first, intergranular layers were not

observed between every grain by STEM analysis, but were identified later by backscattered electron SEM analysis. A typical microstructure is illustrated in Figure 3, in which continuously connected Bi rich boundaries were evident. The thickness of the bright boundaries appeared greater than the intergranular layers previously observed by STEM analysis. This result strongly suggests the presence of an intermediate layer between the grains and the intergranular layer. The width of the intermediate layer was estimated by solving Fick's Second Equation, under the following boundary conditions: The diffusion process can be considered as proceeding from a finite source (Bi), over a finite interval, into an initially undoped (i.e., in this case, zero Bi concentration) $SrTiO_3$ grain, i.e.,

$$\frac{\partial N(d_2,t)}{\partial t} = D \frac{\partial^2 N(d_2,t)}{\partial x^2} \tag{24}$$

$$N(0,t) = N_s$$

$$N(\infty,t) = 0$$

$$N(d_2,0) = 0$$

where, $N(d_2,t)$ is the concentration of the diffusing species; D, the diffusion coefficient; d_2 the diffusion distance from the original interface; t, time; and N_s, the surface concentration. The solution is given by the following equation,

$$N(d_2,t) = N_s \operatorname{erfc} \frac{d_2}{\sqrt{4Dt}} \tag{25}$$

By assuming the thickness d_2 as the distance from surface to the point at which the concentration decreased to 10^{-3} N_s, and taking

a typical[45] ceramic diffusion coefficient of 10^{-14} cm^2/sec

$$d_2 = \sqrt{4(10^{-14})(60 \times 60)(2.32)}$$

$$= 0.3\ \mu m .$$

Based upon ionic radii considerations, Bi^{3+} (1.02 Å) probably substitutes for Sr^{2+} (1.16 Å), rather than for Ti^{4+} (0.61 Å), which has been substantiated by independent measurements.[52] The resulting defect structure would at first suggest additional donor doping (n^+) in the subsurface of the n-type semiconducting grains. Previous discussions (II) were concerned with acceptor compensation of interfacial states, but additional donor doping may also result in an anomalous decrease in conductivity, as illustrated in Figure 39. The conductivity of the intermediate layer is highest at the interface with the grain, and decreases progressively towards the intergranular layer. This is inversely proportional to the Bi concentration, which is preferentially located in the boundary regions, due to the processing conditions employed. Both the grain size and the second firing condition affect the conductivity of the grain, which plays an important role in the high frequency dielectric properties of the IBL capacitor. If the grain size is smaller than the diffusion length of the diffusing species during the second firing stage, all of the grain becomes an intermediate layer, due to diffusion overlap, with the conductivity suddenly decreasing (Figure 39). A small grain size may result in obvious disadvantages for the dielectric properties of IBL capacitor manufactured by these techniques. A decrease in apparent dielectric constant ($\bar{K}'$) and

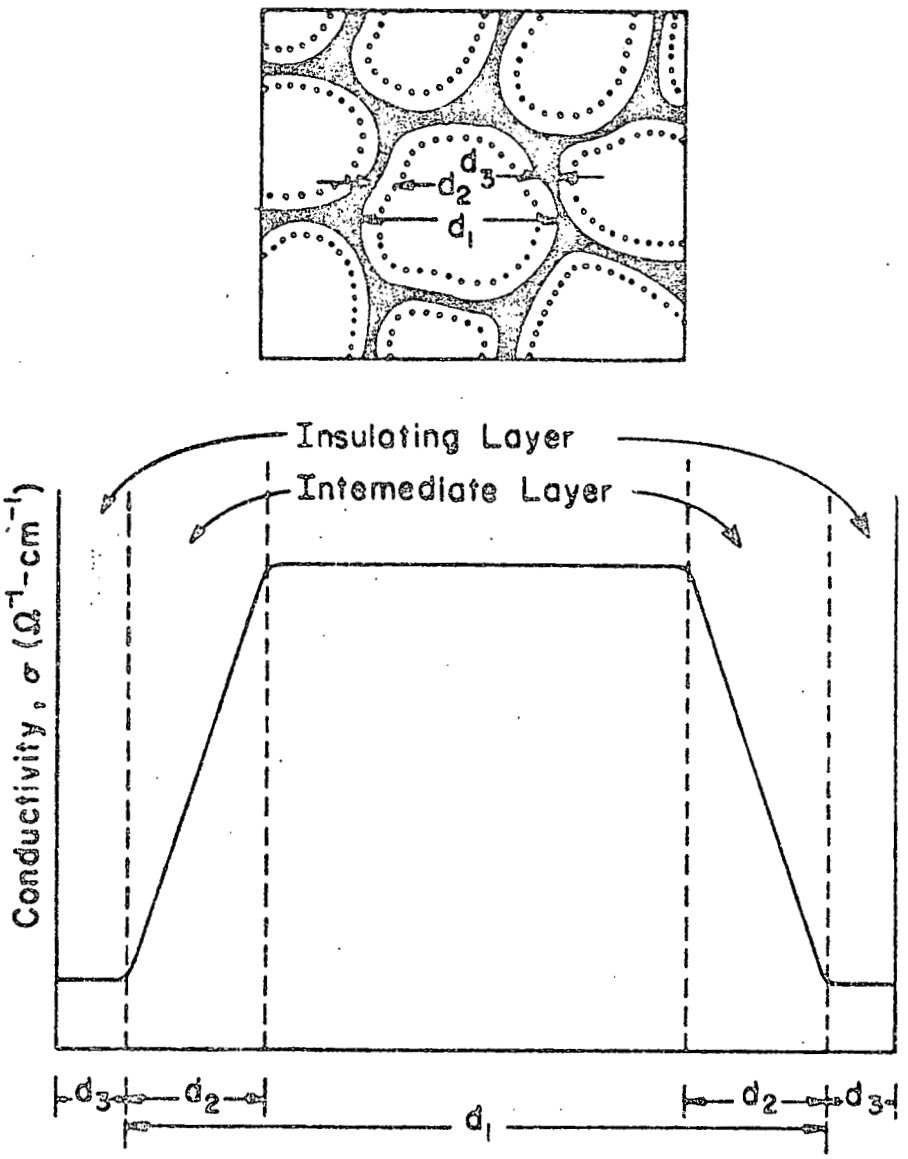

FIGURE 39. Schematic diagram of conductivity for a boundary region.

a low relaxation frequency would result and are discussed in the following section (B).

B. Electrical Properties

1. Current-Voltage Characteristics

The non-ohmic current-voltage behavior of IBL capacitors may be explained in terms of the proposed n-c-i-c-n model. Biased Schottky barriers (i.e., compensated (c) intermediate layers) and insulating (i) intergranular layers, play an important role in the conduction process. Conduction in the low voltage region (Figures 17-19) may be interpreted by Schottky emission or Frenkel-Poole emission, where log I is characteristically proportional to $V^{1/2}$ (Figure 40). Similar results can be found for conduction mechanisms in ZnO varistor (which have a similar microstructure) in the intermediate voltage range.[46-50] For the highly nonohmic region (> 20 volts) several conduction processes have been proposed: including tunneling,[46] space-charge limited current flow [47] and thermionic emission[48]; but it is difficult to determine which process may be responsible for the I-V characteristics in IBL capacitors, in the highly conducting region.

2. Capacitance-voltage Characteristics

Microstructural analysis and current-voltage characteristics demonstrated that the microstructure of IBL dielectrics consisted of semiconducting grains surrounded by continuously connected insulating boundaries. Microstructure-property relation are evident in the capacitance-voltage behavior, illustrated in Figure 21. The dielectric constant of capacitors fabricated

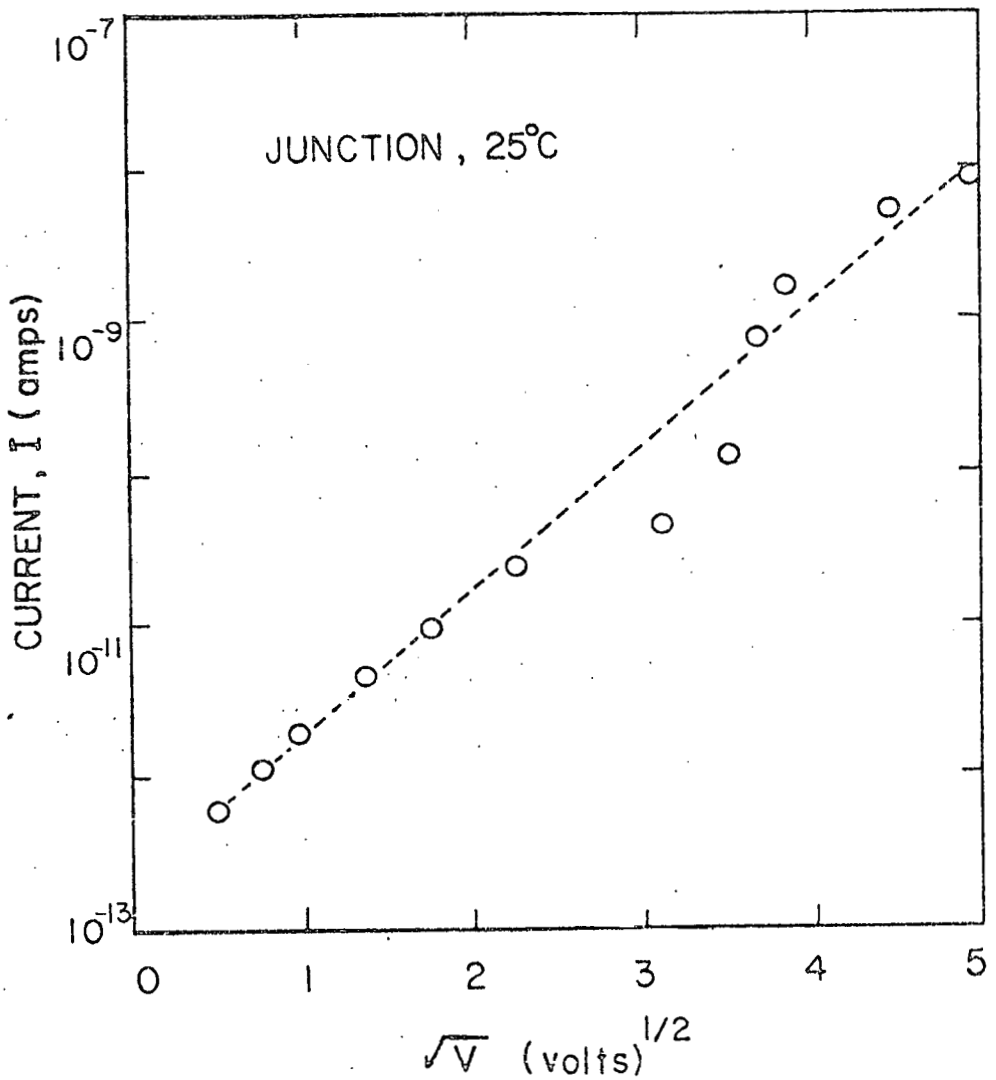

FIGURE 40. Current-voltage characteristics for a single junction in a $SrTiO_3$ IBL capacitor.

with a structure (type I, n-i-n model) were stable with respect to applied voltage; whereas capacitors processed with a 3-layer structure (types G and J, n-c-i-c-n) were voltage sensitive.

The voltage dependent capacitance behavior can be interpreted in terms of the proposed n-c-i-c-n model. On application of a bias voltage, the barrier is lowered ($V_B - V$) in the forward sense, and raised ($V_B + V$) in the reverse case, as illustrated in Figure 41. The total junction capacitance per unit area is given by Equations 5-6. Initially, at V = 0, for a symmetric barrier, $C_C^F = C_C^R$,

$$\frac{1}{\bar{C}} = \frac{2d_3}{\varepsilon_0 K_3} + 2\left[\frac{2V_B}{qN_D+\varepsilon_0 K_2}\right]^{1/2} , \qquad (26)$$

and, finally, at high voltage, $V > V_B$, where the reverse biased capacitance dilutes the total series capacitance,

$$\frac{1}{\bar{C}} = \frac{2d_3}{\varepsilon_0 K_3} + \left[\frac{2(V_B + V)}{qN_D+\varepsilon_0 K_C}\right]^{1/2} \qquad (27)$$

Examination of equations (26-27) in expanded form, indicates why $(\bar{C})^{-2}$ vs. V data (Figure 24) should deviate from linearity, especially at high voltages, due to additional square root terms. Data for single junctions, illustrated in Figure 24, have been analyzed according to the n-c-i-c-n model (Equation 5). An insulation width of 0.1 μm was taken for $2d_3$, which was consistant with STEM analysis of unetched surfaces. The $\bar{K}_2'$ value for linear $SrTiO_3$ was 300. For ferroelectric type G materials, a high field

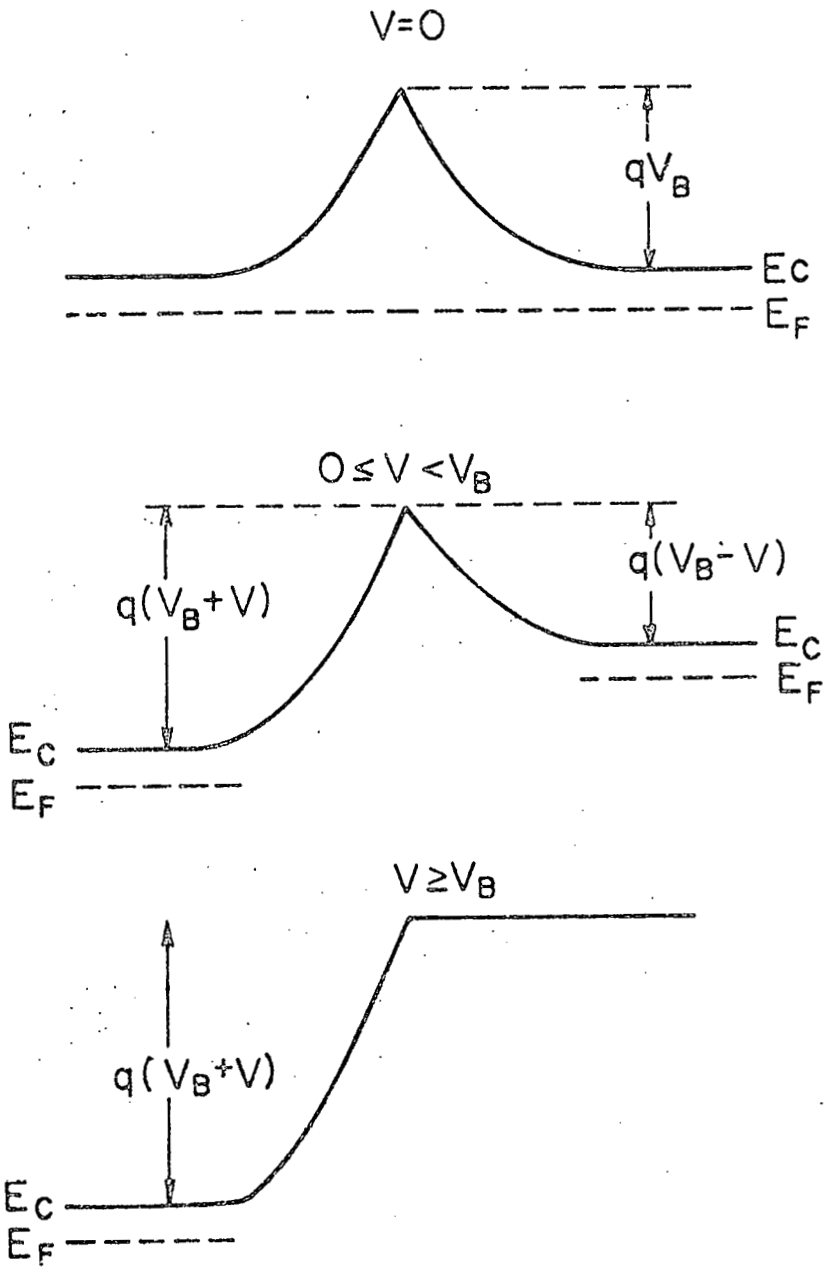

FIGURE 41. Energy band diagram with applied bias voltage for a single junction.

value of $\bar{K}_2'(E) = 600$ was chosen, which is consistent with the saturation behavior of $(Ba,Sr)(Ti,Sn)O_3$. Parameters calculated from intercept and slope data in Figure 24 are summarized in Table 3. These values are in good agreement with cation dopant concentrations (0.3 at.%) in air fired type G material, and combined cation and anion concentrations in reduction fired type J material. Calculated dielectric constants for the insulating boundary phase ($\bar{K}_3'$) are consistant with EPMA and STEM analysis, which identified a titania rich boundary phase in type G material, and bismuth rich boundaries in type J capacitors. It is possible to form insulating second phases in the boundary regions, e.g., $BaO \cdot nTiO_2$ for Type G capacitors; and bismuth-titanate-strontium titanate or bismuth titanate compounds in Type J dielectrics. The calculated values of dielectric constant for the insulating layers ($\bar{K}_3'$) are in good agreement with the values tabulated in Appendix B for the possible compounds. Values of V_B are consistant with calculated activation energies (0.85 eV) from temperature dependent resistivity data (Figure 20). Thus the n-c-i-c-n model for commercial IBL capacitors appears to be extremely relevant, when one considers all the possible variations from ideal representation.

2. Dielectric Dispersion

The microstructures of commercial IBL capacitors can be considered in terms of a three layer structure. Dielectric and electrical measurements indicate the conductivities followed the relationship $\sigma_1 >> \sigma_2 > \sigma_3$, where subscripts 1, 2, and 3 represent: semiconducting grain, intermediate interfacial layer and insulating intergranular layer, respectively. Based on frequency

value of $\bar{K}_2'(E) \doteq 600$ was chosen, which is consistent with the saturation behavior of $(Ba,Sr)(Ti,Sn)O_3$. Parameters calculated from intercept and slope data in Figure 24 are summarized in Table 3. These values are in good agreement with cation dopant concentrations (0.3 at.%) in air fired type G material, and combined cation and anion concentrations in reduction fired type J material. Calculated dielectric constants for the insulating boundary phase ($\bar{K}_3'$) are consistant with EPMA and STEM analysis, which identified a titania rich boundary phase in type G material, and bismuth rich boundaries in type J capacitors. It is possible to form insulating second phases in the boundary regions, e.g., $BaO \cdot nTiO_2$ for Type G capacitors; and bismuth-titanate-strontium titanate or bismuth titanate compounds in Type J dielectrics. The calculated values of dielectric constant for the insulating layers ($\bar{K}_3'$) are in good agreement with the values tabulated in Appendix B for the possible compounds. Values of V_B are consistant with calculated activation energies (0.85 eV) from temperature dependent resistivity data (Figure 20). Thus the n-c-i-c-n model for commercial IBL capacitors appears to be extremely relevant, when one considers all the possible variations from ideal representation.

2. Dielectric Dispersion

The microstructures of commercial IBL capacitors can be considered in terms of a three layer structure. Dielectric and electrical measurements indicate the conductivities followed the relationship $\sigma_1 >> \sigma_2 > \sigma_3$, where subscripts 1, 2, and 3 represent: semiconducting grain, intermediate interfacial layer and insulating intergranular layer, respectively. Based on frequency

TABLE 3

Material Parameters for IBL Capacitors

Type	Material	N_{D^+} (cm^{-3})	$\bar{K}_3'$	V_B (volts)
G	$BaTiO_3$	1.2×10^{18}	55	0.9
J-1	$SrTiO_3$	4.0×10^{20}	102	0.8
J-2	$SrTiO_3$	5.0×10^{20}	39	1.0

dependent dielectric constant plots and corresponding Cole-Cole analysis, the dielectric dispersion behavior for single junctions can be interpreted in terms of the n-c-i-c-n model. Two relaxation processes may occur, one between the grain and the intermediate layer, and the other between the intermediate layer and the intergranular layer. The Maxwell-Wagner model of a dispersive dielectric can be applied to each set of double layers, i.e., n/c and c/i.

Consideration of material properties, $\rho_3 > \rho_2 >> \rho_1$, $d_1 >> d_2 > d_3$ and $K_1' \simeq K_2'$, leads to a simplification of equations 15-19, giving:

$$\tau_{12} = \varepsilon_0 \rho_1 (\bar{K}_1' + \bar{K}_2' \frac{d_1}{d_2}) \qquad (28)$$

$$\tau_{23} = \varepsilon_0 \rho_2 (\bar{K}_2' + \bar{K}_3' \frac{d_2}{d_3}) \qquad (29)$$

For calculations of relaxation frequencies, an insulation layer of 0.1 μm width, and an intermediate layer of 1 μm width, were used. These values were consistent with SEM and STEM analysis. The value of dielectric constant for $SrTiO_3$ and $(Ba,Sr)(Ti,Sn)O_3$ were 300 and 6000, respectively. The latter was a low field value, at 0.01 volts per 0.1 μm (i.e., 10^3 V/cm). Calculated values of $\bar{K}_3'$, taken from C-V analysis (Table 3), were used for the insulating layer. Experimental values of resistivity were taken for the grain and insulating region. A mean resistivity was estimated for the intermediate layer from Figure 39. This was an intermediate value, i.e., between the two end member conditions. That is, ρ_2 was assumed to vary continuously from ρ_1

to ρ_3. Calculated relaxation frequencies (equations 28 and 29) were $f_{12} = 1.8 \cdot 10^7$ and $f_{23} = 1.5 \cdot 10^4$ Hz for $SrTiO_3$ IBLC material J-1. They were in good agreement with experimental Cole-Cole data, i.e., $1.5 \cdot 10^7$ Hz and $1.0 \cdot 10^5$ Hz, respectively. Calculated relaxation frequencies for G and J-2were also in good agreement with experimental data, and are summarized in Table 4. Note: τ_{12} values are much smaller than τ_{23} values, and τ_{12} indicates a higher frequency relaxation. The distribution factor, α, for the higher frequency relaxation, is less than the α values at low frequency. These results suggest the Maxwell-Wagner relaxation is more pronounced at the semiconducting-intermediate layer interface, than at the intermediate layer-insulating interface, which was to be expected. The conductivity of the grain is the most important criteria in the dielectric dispersion behavior of IBL dielectrics. The higher the conductivity, the greater the dispersion frequency, as predicted from equation 28.

Dielectric dispersion behavior of polycrystalline specimens (with a n-c-i-c-n structure) differ somewhat from measurements on single junctions. The resistance of bulk specimens can be summed from a series connection of single junctions, which results in a higher apparent resistivity. The insulating layer capacitance dominates the weak field range (Figure 19). Dielectric dispersion behavior of bulk polycrystalline type G IBL capacitors, exhibit a typical Debye relaxation, and the relaxation frequency (10^6 Hz) can be estimated from $\bar{K}'$ vs. frequency plots. The relaxation frequency can also be obtained from Cole-Cole plots, in which the distribution coefficient is very low, i.e., $\alpha = 0.03$. Calculated dispersion parameters ($K_s' = 55{,}000$,

TABLE 4

Material Properties for a Single Junction

Measured	Calculated
K_1 = 6000 $BaTiO_3$ (G)	
d_1 = 50 μm, ρ_1 = 50 Ω-cm, $f_{12} = 5 \cdot 10^5$ Hz	$\rho_2 = 10^5$, $f_{12} = 1.2 \times 10^5$ Hz
d_2 = 1.0 μm	
d_3 = 0.1 μm, $\rho_3 = 10^{10}$ Ω-cm, $f_{23} = 1 \cdot 10^4$ Hz	$K_3' = 55$, $f_{23} = 2.7 \times 10^3$ Hz
K_2 = 300 $SrTiO_3$ (J-1)	
d_1 = 30 μm, ρ_1 = 30 Ω-cm, $f_{12} = 1.5 \cdot 10^7$ Hz	$\rho_2 = 10^5$, $f_{12} = 1.8 \cdot 10^7$ Hz
d_2 = 1.0 μm	
d_3 = 0.1 μm, $\rho_3 = 10^{10}$ Ω-cm, $f_{23} = 1.0 \cdot 10^5$ Hz	$K_3' = 102$, $f_{23} = 1.5 \times 10^4$ Hz
K_2 = 300 $SrTiO_3$ (J-2)	
d_1 = 30 μm, ρ_1 = 30 Ω-cm, $f_{12} = 5.0 \cdot 10^7$ Hz	$\rho_2 = 10^5$, $f_{12} = 4.1 \cdot 10^7$ Hz
d_2 = 1.0 μm	
d_3 = 0.1 μm, $\rho_3 = 10^{10}$ Ω-cm, $f_{23} = 5.0 \cdot 10^4$ Hz	$K_3' = 39$, $f_{23} = 2.6 \cdot 10^4$ Hz

$K_\infty' = 6{,}000$, $\tau_K = 2.4 \times 10^{-7}$, $f_K = 6.5 \times 10^5$ Hz) are in good agreement with experimental data (Figures 31 and 34). The dispersion characteristics of $SrTiO_3$ type J-1 and J-2 polycrystalline capacitors were weak in the mega Hz range. Further studies are needed at higher frequencies (> 100 MHz) for the dielectric dispersion characteristics of $SrTiO_3$ IBL capacitors.

For the experimental two layer structures, type I capacitors (i.e., n-i-n), relaxation frequencies were calculated from the following expression,

$$\tau = \varepsilon_0 \rho_1 K_2' \frac{d_1}{d_3} \quad , \tag{30}$$

and were $2.7 \cdot 10^7$ Hz and $5 \cdot 10^7$ Hz respectively, for types J-1 and J-2 capacitors; which are in good agreement with experimental values (Figures 37 and 38).

It is interesting to note, that in the three-layer model (n-c-i-c-n), the low distribution coefficient (α) for the Cole-Cole arc at high frequencies probably indicates a step junction between the conducting grains and the intermediate compensation layer, whereas, the high distribution coefficient at low frequencies, indicates a graded or diffuse junction, between the insulating layer and the compensation layer, which is to be expected from the diffusion processes involved in the processing.

SUMMARY

1. The ceramic microstructures of internal boundary layer capacitors based upon $BaTiO_3$ and $SrTiO_3$ were characterized. Commercial capacitors had a grain size of 20-60 μm, and contained a continuously connected boundary phase.

2. The chemical composition of the boundary region was different from the grains; the boundary region consisted of an intermediate interfacial (compensation) layer between the grain and the intergranular layer. The interfacial layer formed by diffusion processes during the second firing stage.

3. The intrinsic properties of individual grains and boundary regions were determined by microscale electrical measurements. The grains were semiconducting, with typical resistivities of $10\text{-}10^2$ Ω-cm; and the boundary regions were insulating, typically $10^{10}\text{-}10^{11}$ Ω-cm.

4. The conductivity of the intermediate interfacial layer decreased progressively with compensation of the donors.

5. Commercial IBL capacitors fabricated by a two step infiltration process were voltage sensitive; and C^{-2} vs. V characteristics indicated the electrical behavior of the intermediate layer to be similar to that of a depletion layer.

6. Experimental fine grain IBL capacitors, developed by microstructural engineering techniques (i.e., liquid phase sintering of conducting particles), only contained an insulating boundary

phase, and this microstructure could be approximated by a simple n-i-n model. These capacitors were extremely stable with respect to voltage and temperature, and were suitable for multilayer capacitors.

7. Dielectric dispersion behavior of single junctions in large grain commercial IBL capacitors, were explained in terms of two relaxation processes. The resistivity of the semiconducting grains played an important role in the dielectric dispersion behavior.

8. A hybrid representation of ceramic microstructure was proposed for commercial capacitors, and their properties explained in terms of a n-c-i-c-n model. Capacitance-voltage characteristics and dielectric dispersion behavior were interpreted in terms of a three-layer equivalent circuit.

REFERENCES

1. S. M. Park, Liquid Phase Sintering of Heterophasic Dielectrics, Ph.D. Thesis: University of Illinois (1977).
2. J. Volger, "Some Properties of Lanthanum and Strontium Magnetites," Semiconductor Materials, Butterworth (1951) 162.
3. Ya. M. Ksendzov, "Electrical Properties of Titanium Dioxide," J. Tech. Phys., U.S.S.R. 20 (1950) 117.
4. F. C. Brockman, P. A. Dowling, and W. G. Steneck, "Dimensional Effects Resulting from a High Permittivity Found in a Ferromagnetic Ferrite," Phys. Rev. 77 (1950) 85.
5. C. G. Koops, "On the Dispersion of Resistivity and Dielectric Constant of Some Semiconductors at Audio Frequencies," ibid, 83 (1951) 121.
6. A. Fairweather, and E. J. Frost, "Dielectric Behavior of Granular Semiconductor Aggregates," Proc. I.E.E. No. 1486, Mar. 1953, 15.
7. Ya. M. Ksendzov, "Electrical Properties of Titanium Dioxide," J. Tech. Phys. 20 (1950) 117.
8. J. Daniel and K. H. Härdtl, "Electrical Conductivity at High Temperature of Donor-Doped Barium Titanate Ceramics," Phillips Res. Repts. 31 (1976) 489.
9. H. Brauer, "Korngrenzensporrschichten in $BaTiO_3$-Keramik mit hoher effekt:ver kielektrizitatskonstante," Z. Angew. Phy. 29 (1970) 282.

10. H. Ikushima, and S. Hayakawa, "Electrical Properties of Ag-Doped Barium Titanate Ceramics," Jap. J. Appl. Phys. 4 No. 5 (1962) 328.

11. O. Saburi, "Semiconducting Bodies in the Family of Barium Titanates," J. Am. Cer. Soc. 44 (1961) 54.

12. P. Gerthsen and K. M. Hardtl, "Method for Proof of Inhomogeneity of Conduction at Grain Boundaries," Z. Naturforsch 18a (1963) 423.

13. W. Heywang, "Semiconducting Barium Titanate," J. Mat. Sci. 6 (1971) 1214.

14. H. Veoka, "The Doping Effects of Transition Elements on the PTC Anomaly of Semiconductive Ferroelectric Ceramics," Ferroelectrics 7 (1974) 351.

15. T. Murakami, T. Miyashita, M. Nakahara, and E. Sekine, "Effect of Rare-Earth Ions on Electrical Conductivity of $BaTiO_3$ Ceramics," J. Am. Cer. Soc. 56 (1973) 294.

16. Y. Matsuo, M. Fujimura, H. Sasaki, K. Nagase, S. Hayakawa, "Semiconducting $BaTiO_3$ with Additions of Al_2O_3, SiO_2 and TiO_2," Bull. Am. Cer. Soc. 47 (1968) 292.

17. M. Kahn, "Effect of Heat-Treatment on the PTCR Anomaly in Semiconducting Barium Titanate," Bull. Am. Cer. Soc. 50 (1971) 676.

18. W. Heywang, "Anomalous Semiconductor Effects in $BaTiO_3$," Solid State Phys. 4 (1960) 877.

19. W. Heywang, "Barium Titanate as a Semiconductor with Blocking Layers," Solid State Elec. 3 (1) (1961) 51.

20. W. Heywang, "Resistivity Anomaly in Doped Barium Titanate," J. Am. Cer. Soc. 47 (1964) 484.

21. G. H. Jonker, "Halogen Treatment of Barium Titanate Semiconductors," Mat. Res. Bull. 2 (1967) 401.

22. J. Daniels and R. Wernicke, "New Aspect of an Improved PTC Model," Phillips Res. Repts. 31 (1976) 489.

23. R. Wernicke, "A Two Layer Model Explaining the Properties of $SrTiO_3$ Boundary Layer Capacitors," to be published in Advances in Ceramics (1981).

24. R. Wernicke, "Formation of Second Phase Layers in $SrTiO_3$ Boundary Layer Capacitors," to be published in Advances in Ceramics (1981).

25. T. Vojnovich and T. D. McGee, "Determination of Donor Gradients within Surface Barriers Formed on Dense Gd-Doped Barium Titanates," J. Am. Cer. Soc. 52 (1969) 386.

26. H. Rehme, "Elektronenmikroskopischer Nachweis von Sperrschichten in Bariumtitanat-Kaltleiter-Keramic," Phy. Stat. Sol. 18 (1966) K101.

27. P. Gerthsen and B. Hoffmann, "Current-Voltage Characteristics and Capacitance of Single Grain Boundaries in Semiconducting $BaTiO_3$ Ceramics," Sol. Stat. Elec. 16 (1973) 617.

28. P. F. Bongers and P. E. C. Franken, "Secondary Phases and Segregation Layers at Grain Boundaries in Electronic Ceramic Materials," to be published in Advances in Ceramics (1981).

29. British Patent 1204436 (1967).

30. British Patent 1454181 (1973).

31. T. Edahiro and F. Yoshimura, "Experiments on Boundary Layer Dielectrics with Low Temperature Coefficients," Rev. Elec. Comm. Lab. 21 (1973) 843.

32. S. Waku, "Studies on the Boundary Layer Ceramic Capacitor," Rev. Elec. Comm. Lab., 15 (1967) 689.

33. J. C. Maxwell, A Treatise on Electricity and Magnetism, Clarendon Press, Oxford (1892).

34. K. W. Wagner, Arch. fur Electrotech 2 (1914) 371, cited by Sillars, R. W., J. I. E. E. (London) 80 (1937) 378.

35. K. S. Cole and R. H. Cole, "Dispersion and Adsorption in Dielectrics," J. Chem. Phys. 9 (1941) 341.

36. N. E. Hill, W. E. Vaughan, A. H. Pricé and M. Davies, Dielectric Properties and Molecular Behavior, Van Nostrand Reinhold Co. London (1969).

37. R. H. Cole and D. W. Davison, "Dielectric Relaxation in Glycerine," J. Chem. Phys. 18 (1950) 1417.

38. R. B. Hilborn, Jr., Conductivity and Dielectric Losses in Sintered Ceramic Compacts of Ferric Oxide, Ph.D. Thesis: The Pennsylvania State University (1964).

39. D. A. Payne, The Role of Internal Boundary Layers upon the Dielectric Properties of Polycrystalline Ferroelectric Materials, Ph.D. Thesis: The Pennsylvania State University (1973).

40. B. A. Tuttle, Dielectric Dispersion Analysis of Zinc Oxide Based Ceramic Varistors, M.S. Thesis: University of Illinois (1977).

41. A. V. Turik, K. R. Chernyshov, and V. D. Komarov, "Dielectric Dispersion in Ferroelectrics with Perovskite Structure over the Meter-Wave Range," Ferroelectrics 6 (1973) 45.

42. S. Waku, M. Uchidate and K. Kiuchi, "Studies on the (Ba,Sr) TiO_3 Boundary Layer Ceramic Dielectrics," Rev. Elec. Comm.

Lab. 18 (1970) 681.

43. H. Park and D. A. Payne, "Characterization of Internal Boundary Layer Capacitors," to be published in Advances in Ceramics (1981).

44. J. Volger, Progress in Semiconductor, ed. A. F. Gibson, John Wiley and Sons, Inc., N.Y., N.Y., 4 (1960) 207.

45. W. D. Kingery, H. K. Bowen and D. R. Uhlmann, "Introduction to Ceramics," 2nd Ed., John Wiley and Sons, Inc., N.Y., N.Y. 240.

46. L. M. Levinson and H. R. Phillip, "The Physics of Metal Oxide Varistors," J. Appl. Phys. 46, (1975) 1332.

47. V. A. Vulcan, "Characterization and Analysis of Polycrystalline Semiconducting ZnO Screened Capacitor Family," IEEE Proc. Elect. Comp. Conf. S, (1966) 296.

48. C. H. Seager and G. E. Pike, "Grain Boundary States and Varistor Behavior in Silicon Bicrystals," Appl. Phys. Lett. 35 (1979) 709.

49. W. G. Murris, "Physical Properties of the Electrical Barriers in Varistors," J. Vac. Sci. Tech. 13 (1976) 926.

50. K. Eda, "Conduction Mechanism of Non-Ohmic Zinc Oxide Ceramics," J. Appl. Phys. 49 (1978) 2964.

51. T. Negas, R. S. Roth, H. S. Parker, and D. Minor, J. Sol. State Chem., 9 (1974) 300.

52. A.K. Methrotra and D.A.Payne, to be published.

APPENDIX A

Phase Diagram for the $BaO-TiO_2$ System[51]

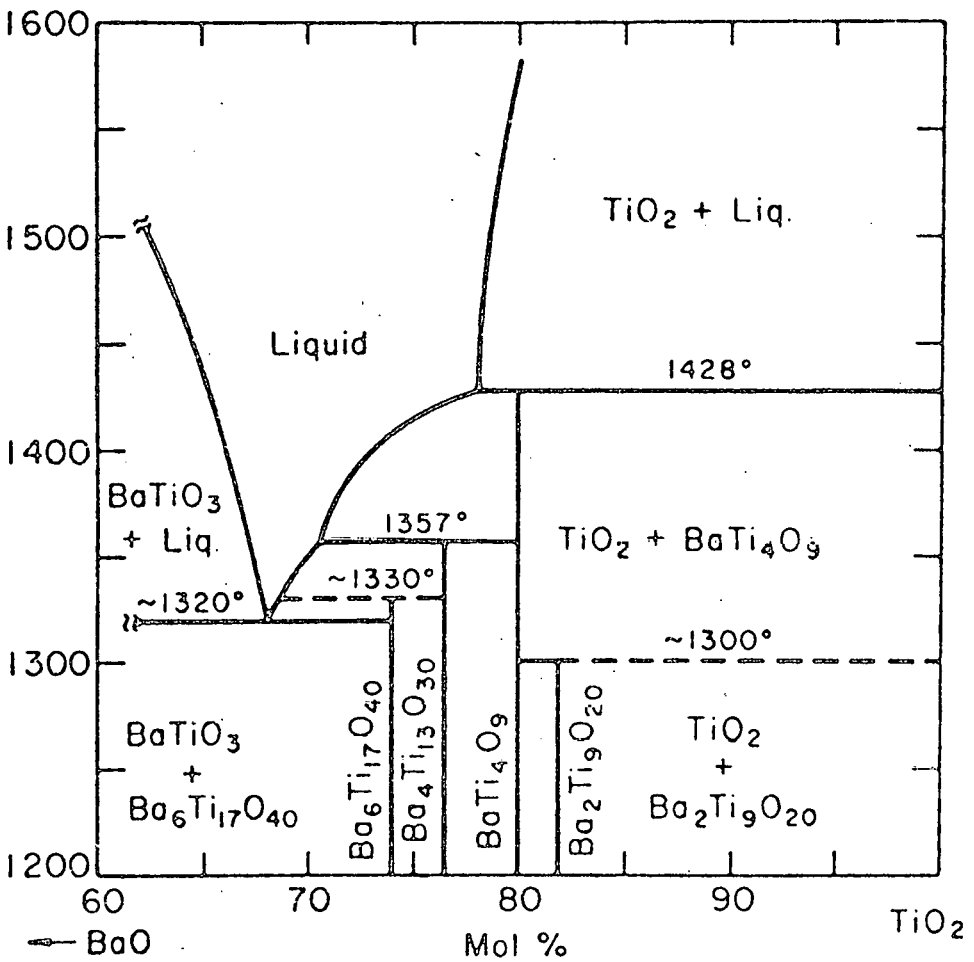

APPENDIX B

Dielectric Constants of Several $SrO-Bi_2O_3-TiO_2$ Compounds

Compound	Dielectric Constant, $\bar{K}'$	Temperature (°C)
$Bi_4Ti_3O_{12}$	18	$0 < T < 550$
$SrBi_4Ti_4O_{15}$	190	$0 < T < 300$
$Sr_2Bi_4Ti_5O_{18}$	280	$T < 100$
$Bi_2Ti_4O_{11}$	40 ~ 60	$T < 100$
$(1-2)SrTiO_3-x/3\ Bi_2O_3 \cdot 3TiO_2$	20 ~ 800	$-50 < T < 50$

APPENDIX C

Equivalent Circuits for a Three Layer n-c-i-c-n Structure

The composite admittance ($\bar{Y}$) of series connected layers follows:

$$\bar{Y} = \frac{Y_1 Y_2 Y_3}{Y_1 Y_2 + Y_2 Y_3 + Y_{13}} \tag{C1}$$

where

$$\bar{Y} = \frac{1}{\bar{R}} + i\omega\bar{C}$$

$$Y_1 = \frac{1}{R_1} + i\omega C_1$$

$$Y_2 = \frac{1}{R_2} + i\omega C_2$$

$$Y_3 = \frac{1}{R_3} + i\omega C_3$$

Substitution of Y_1, Y_2 and Y_3 into equation C1 gives

$$\bar{Y} = \frac{[1-\omega^2(R_1R_2C_1C_2+R_1R_3C_1C_3+R_2R_3C_2C_3)][R_1+R_2+R_3-\omega^2R_1R_2R_3(C_1C_2+C_2C_3+C_1C_3)]}{[R_1+R_2+R_3-\omega^2R_1R_2R_3(C_1C_2+C_2C_3+C_1C_3)]^2}$$

$$+ \frac{i\omega\{(R_1C_1+R_2C_2+R_3C_3-\omega^2R_1R_2R_3C_1C_2C_3)[R_1+R_2+R_3-\omega^2R_1R_2R_3(C_1C_2+C_2C_3+C_1C_3)]}{[R_1+R_2+R_3-\omega^2R_1R_2R_3(C_1C_2+C_2C_3+C_1C_3)]^2}$$

From equation C2 the following electrical parameters can be derived

$$\bar{R} = \frac{(R_1+R_2+R_3)^2+\omega^2(R_1^2R_2^2C_2^2+R_1^2R_3^2C_3^2+R_1^2R_2^2C_1^2+R_2^2R_3^2C_3^2+2R_1R_2R_3^2C_3^2+}{(R_1+R_2+R_3)+\omega^2(R_1^2R_2C_1^2+R_1^2R_3C_1^2+R_1R_2^2C_2^2+R_1R_3^3C_3^3+R_2R_3^2C_3^2+R_2R_3^2C_2C_3)}$$

$$+\omega^2[R_1C_1+R_2C_2+R_3C_3-\omega^2R_1R_2R_3C_1C_2C_3][R_1R_2C_2+R_1R_3C_3+R_1R_2C_1+R_2R_3C_3+R_1R_3C_1+R_2R_3C_2]$$

$$+\qquad\qquad\omega^2(R_1R_2C_2+R_1R_3C_3+R_1R_2C_1+R_2R_3C_3+R_1R_3C_1+R_2R_3C_2)^2$$

$$-[1-\omega^2(R_1R_2C_1C_2+R_1R_3C_1C_3+R_2R_3C_2C_3)][R_1R_2C_2+R_1R_3C_3+R_1R_2C_1+R_2R_3C_3+\ R_1R_3C_1+R_2R_3R_2]\}$$

$$+\qquad\qquad\omega^2(R_1R_2C_2+R_1R_3C_3+R_1R_2C_1+R_2R_3C_3+R_1R_3C_1+R_2R_3C_2)^2$$

$$R_3^2R_1^2C_1^2+R_2^2R_3^2C_2^2+2R_1^2R_2C_1C_2+2R_1R_2^2R_3C_2^2+2R_1^2R_3^2C_1C_3+2R_1^2R_2R_3C_1^2+2R_2^2R_3^2C_2C_3)+$$

$$+\qquad\qquad\omega^4(R_1^2R_2^2R_3C_1^2C_2^2+R$$

$$\left|\frac{\omega^4 R_1^2 R_2^2 R_3^2 (C_1C_2+C_2C_3+C_1C_3)^2}{2R_3^2C_2^2C_3^2+R_1^2R_2R_3^2C_1^2C_3^2)}\right. \tag{C3}$$

(C2)

$$\bar{C} = \frac{(R_1^2C_1+R_2^2C_2+R_3^2C_3)+\omega^2(R_1^2R_2^2C_1C_2^2+R_2^2R_3^2C_2^2C_3+R_1^2R_2^2C_1^2C_2 + }{(R_1+R_2+R_3)^2+\omega^2(R_1^2R_2^2C_2^2+R_1^2R_3^2C_3^2+R_1^2R_2^2C_1^2+R_2^2R_3^2C_3^2+2R_1R_2R_3^2C_3^2+R_3^2}$$

The static limits ($\omega = 0$) on the frequency dependent terms are:

$$\bar{R}_s = R_1 + R_2 + R_3 \tag{C5}$$

$$\bar{C}_s = \frac{R_1^2C_1+R_2^2C_2+R_3^2C_3}{(R_1+R_2+R_3)^2} \tag{C6}$$

and at infinite frequency ($\omega = \infty$)

$$\bar{R}_\infty = \frac{R_1R_2R_3(C_1C_2+C_2C_3+C_1C_3)}{R_1R_2C_1C_2+R_1R_3C_1C_3+R_2R_3C_2C_3} \tag{C7}$$

$$\bar{C}_\infty = \frac{C_1C_2C_3}{C_1C_2+C_2C_3+C_1C_3} \tag{C8}$$

In terms of material properties (K', ρ)

$$\bar{\rho}_s = (\rho_1d_1 + \rho_2d_2 + \rho_3d_3)/d \tag{C9}$$

$$\bar{K}'_s = d\left[\frac{\rho_1^2d_1K'_1+\rho_2^2d_2K'_2+\rho_3^2d_3K'_3}{(\rho_1d_1+\rho_2d_2+\rho_3d_3)^2}\right] \tag{C10}$$

$$\frac{}{R_3^2}\ \frac{R_1^2R_3^2C_1C_3^2+R_1^2R_3^2C_1^2C_3+R_2^2R_3^2C_2C_3^2)}{R_1^2C_1^2+R_2^2R_3^2C_2^2+2R_I^2R_2^2C_1C_2+2R_1R_2^2R_3C_2^2+2R_1^2R_3^2C_1C_3+2R_1^2R_2R_3C_1^2+2R_2^2R_3^2C_2C_3+\omega^4R_1}+$$

$$+ \quad \frac{\omega^4 R_2^2 R_3^2 C_1 C_2 C_3 (C_1 C_2 + C_2 C_3 + C_1 C_3)}{R_3^2 (C_1 C_2 + C_2 C_3 + C_1 C_3)^2} \qquad \text{(C4)}$$

$$\frac{}{R_1^2 R_2^2}$$

$$\bar{\rho}_{\infty} = \frac{1}{d}\left[\frac{\rho_1\rho_2\rho_3(K_2'K_3'd_1+K_1'K_3'd_2+K_1'K_2'd_3)}{\rho_1\rho_2K_1'K_2'+\rho_1\rho_3K_1'K_3'+\rho_2\rho_3K_2'K_3'}\right] \tag{C11}$$

$$\bar{K}_{\infty}' = \frac{dK_1'K_2'K_3'}{d_1K_2'K_3'+d_2K_1'K_3'+d_3K_1'K_2'} \tag{C12}$$

SUGGESTIONS FOR FUTURE WORK

1. A model was proposed to explain the microstructure-property relations for IBL capacitors. To further substantiate this model, further microstructural analysis is suggested, especially of the physical and chemical nature of the boundary conditions.

2. Additional development of a multilayer IBL capacitor is recommended, with the expressed purpose of developing fine grain microstructures.

3. The nature of ceramic microstructure and related electrical properties of semiconducting/insulating ceramics should be reinvestigated, especially with respect to ZnO based varistors and PTCR $BaTiO_3$ thermistors.

VITA

Hyun Duk Park was born on [redacted]. He attended Whimoon High School and Hanyang University in Seoul. Upon receiving his Bachelor of Science degree in Ceramic Engineering in February, 1974, he joined the Ceramic Materials Laboratory of the Korean Institute of Science and Technology, and worked on electronic ceramics and refractory materials. In August 1977, he entered the graduate program at the University of Illinois, where he received a Master of Science degree in Ceramic Engineering in December 1978.